J. Fluid Mech. (1995), *vol.* 301, *pp.* 295–324

Transverse motion of a disk through a rotating viscous fluid

By JOHN P. TANZOSH AND H. A. STONE

Division of Applied Sciences, Harvard University, Cambridge, MA 02138, USA

(Received 27 June 1994 and in revised form 19 June 1995)

A thin rigid disk translates edgewise perpendicular to the rotation axis of an unbounded fluid undergoing solid-body rotation with angular velocity Ω. The disk face, with radius a, is perpendicular to the rotation axis. For arbitrary values of the Taylor number, $\mathscr{T} = \Omega a^2/\nu$, and in the limit of zero Reynolds number $\mathscr{R}_e$, the linearized viscous equations reduce to a complex-valued set of dual integral equations. The solution of these dual equations yields an exact representation for the velocity and pressure fields generated by the translating disk.

For large rotation rates $\mathscr{T} \gg 1$, the $O(1)$ disturbance velocity field is confined to a thin $O(\mathscr{T}^{-1/2})$ boundary layer adjacent to the disk. Within this boundary layer, the flow field near the disk centre undergoes an Ekman spiral similar to that created by a nearly geostrophic flow adjacent to an infinite rigid plate. Additionally, flow within the boundary layer drives a weak $O(\mathscr{T}^{-1/2})$ secondary flow which extends parallel to the rotation axis and into the far field. This flow consists of two counter-rotating columnar eddies, centred over the edge of the disk, which create a net in-plane flow at an angle of 45° to the translation direction of the disk. Fluid is transported axially toward/away from the disk within the core of these eddies. The hydrodynamic force (drag and lift) varies as $O(\mathscr{T}^{1/2})$ for $\mathscr{T} \gg 1$; this scaling is consistent with the viscous stresses created in the Ekman boundary layer. Additionally, an approximate expression, suitable for all Taylor numbers, is given for the hydrodynamic force on a disk translating broadside along the rotation axis and edgewise transverse to the rotation axis.

1. Introduction

There exist few analytical solutions describing particle motion transverse to the rotation axis of a fluid in solid-body rotation. Such motions occur in centrifugal separations and swirling flows of particle-laden fluids. The analysis of such problems is difficult owing to the three-dimensional character of the disturbance flow field created by a moving particle. To further the theoretical understanding in this problem area, we present an exact solution for the velocity and pressure fields created by the edgewise translation of a circular disk transverse to the rotation axis.

Consider a thin disk of radius a translating with velocity $\boldsymbol{U}_p$ through a fluid in solid-body rotation with angular velocity Ω. The plane of the disk is perpendicular to the rotation axis, and the disk translates in the edgewise direction (figure 1). The fluid motion is characterized by two dimensionless parameters: the Reynolds number $\mathscr{R}_e = |\boldsymbol{U}_p|a/\nu$ and the Taylor number $\mathscr{T} = \Omega a^2/\nu$, where ν denotes the kinematic viscosity of the fluid. We study the limit where the Reynolds number $\mathscr{R}_e \ll 1$, so that

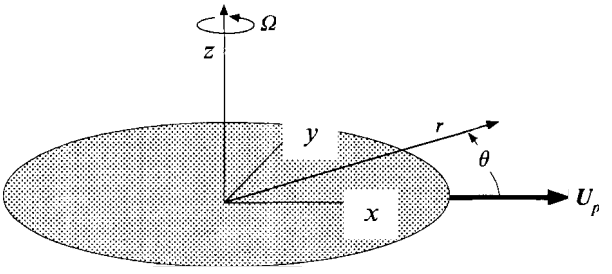

FIGURE 1. Disk translating edgewise through an unbounded fluid undergoing solid-body rotation with angular velocity Ω. The z-axis is aligned parallel to the rotation axis, and the disk translates along the x-direction.

Investigation	Disk motion
Ray (1936)	**broadside/edgewise**, in-plane rotation; $\mathscr{T} = 0$
Davis (1991; 1993)	**broadside/edgewise** translation near walls; $\mathscr{T} = 0$
Moore & Saffman (1969*a*,*b*)	**broadside/edgewise**; rotating fluids $\mathscr{T} \gg 1$
Hocking *et al.* (1979)	**broadside**; in a long container $\mathscr{T} \gg 1$
Vedensky & Ungarish (1994)	**broadside**; bounded/unbounded; all $\mathscr{T}$
Ungarish & Vedensky (1995)	
Here	**edgewise** motion; unbounded; all $\mathscr{T}$

TABLE 1. Research related to the edgewise translation of a disk in a Stokes ($\mathscr{T} = 0$) or rotating viscous flow and formulated using dual integral equations.

the convective acceleration effects may be neglected, and obtain an exact solution, valid for any Taylor number, for the linearized equations governing rotating viscous flows. To our knowledge, this is the first solution to describe transverse particle motion at arbitrary rotation rates.

The mathematical procedures employed here reduce the linearized governing equations to a set of dual integral equations. Table 1 summarizes related research in which dual integral equation formulations describe the motion of a disk either in a Stokes flow or through a fluid in solid-body rotation. In particular, Ray (1936) and Davis (1991) analysed the edgewise translation of a circular disk in an unbounded Stokes flow ($\mathscr{T} = 0$); Moore & Saffman (1969*a*,*b*) considered broadside and edgewise translation of a disk through a rotating fluid in the rapid rotation limit ($\mathscr{T} \gg 1$) by examining the appropriate boundary layer equations; and Vedensky & Ungarish (1994) and Ungarish & Vedensky (1995) investigated broadside motion along the rotation axis through unbounded and bounded geometries at arbitrary Taylor number. Tanzosh (1994) and Tanzosh & Stone (1995) present a general approach for analysing a variety of disk motions including the Stokes flow problem, the transverse translation of a disk perpendicular to the rotation axis, the broadside motion of a disk parallel to the rotation axis, and the in-plane rotation of a disk along an axis parallel to the rotation axis.

Solid-body rotation produces a number of interesting and often surprising effects on the structure of the flow field caused by transverse particle motion. For fluids in rapid rotation so that $\mathscr{T} \gg 1$ but $\mathscr{R}_e\mathscr{T}^{-1} = |\boldsymbol{U}_p|/\Omega a \ll 1$, the flow field tends toward having a two-dimensional structure. The mathematical statement describing this inviscid flow limit is the Taylor–Proudman theorem, which states that the fluid velocity $\boldsymbol{u}$ satisfies $\boldsymbol{\Omega} \cdot \nabla \boldsymbol{u} = \boldsymbol{0}$. Thus, disturbances generated by particle motion, or perhaps by topological disturbances to an imposed flow, have long-range effects in

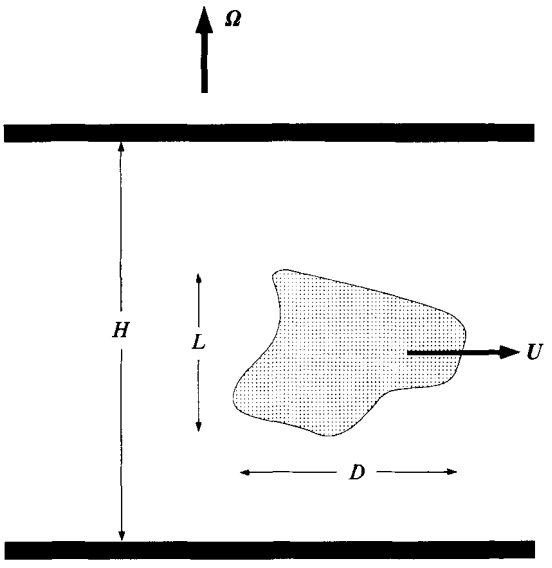

FIGURE 2. Geometric length scales of a particle translating between rigid walls in a fluid undergoing solid-body rotation.

directions parallel to the rotation axis. The classic example of this effect is the Taylor column in which a circumscribing column of fluid accompanies a translating particle. The review articles by Hide (1966), Lighthill (1966) and Bush, Stone & Tanzosh (1995) and the text by Greenspan (1968) discuss some of the physical features of this type of motion.

Table 2 summarizes experimental work related to the motion of a particle transverse to the rotation axis. The experiments demonstrate that in rapidly rotating fluids, translating 'fat bodies' tend to block fluid from entering a cylindrical region circumscribing the particle and extending parallel to the rotation axis (e.g. Taylor 1923; Hide & Ibbetson 1968). This phenomenon is termed Taylor blocking. 'Thin objects', however, do not block the flow (see experiments by Maxworthy 1969 and Vaziri & Boyer 1971); instead, streamlines pass through the circumscribing cylinder at a deflected angle described analytically by Moore & Saffman (1969*a*).

Hide & Ibbetson (1966) recognized that Taylor blocking arises when the length of the particle in the direction of the rotation axis is sufficiently large. In the absence of rotation, translating 'fat bodies' create velocity variations in all directions. However, in rapidly rotating flows, velocity gradients parallel to the rotation axis are inhibited, and instead fluid is blocked from entering a cylindrical region circumscribing and moving with the particle. 'Thin bodies', on the other hand, displace a small fluid volume and so may not create a sufficiently strong vertical disturbance for the Taylor–Proudman constraint to modify the flow field in such a dramatic manner.

Hide & Ibbetson (1966) argued that convective inertial influences, whose magnitude relative to the Coriolis force is measured by the Rossby number $\mathscr{R}_o = \mathscr{R}_e\, \mathscr{T}^{-1}$, of sufficient strength will disrupt Taylor blocking. Specifically, in a bounded flow, Taylor blocking should occur provided the ratio of the height of the particle L to the channel depth H (see figure 2) satisfies $L/H > \alpha\, \mathscr{R}_o$, where α is an $O(1)$ constant. Hide & Ibbetson (1966) also performed experiments which were in reasonable agreement with this criterion. We thus might expect that the classic Taylor blocking phenomenon may not occur for the transverse motion of an infinitely thin disk, although rotation

Researcher	$\mathscr{R}_e$	$\mathscr{R}_o$	$\mathscr{T}$	D/L	H/L	Comment
Taylor (1923)						blocking
Hide & Ibbetson (1966)	7–100	0.003–0.02	10^2–10^4	0.6	4	description; blocking/deflection
Hide & Ibbetson (1968)		0.002–0.02	50–750	1	12	Taylor column bending; inertial effects
Vaziri & Boyer (1971)	120	0.04	3000	0.0625	5	shallow topography; deflection
Davies (1972)	25	0.01	2500	1	8	description of interior flow
Mason (1975)		0.001–1.0	25–250	1	3–20†	blocking/deflection; drag/lift
Moore & Saffman (1969)		0.012	2150	400	5600	disk; streamline deflection
Karanfilian & Kotas (1981)	0.03–3300	0.24–20	0.08–300	1	34	free motion of particle; lift/drag

TABLE 2. Experimental studies related to the slow translation of a particle in a direction perpendicular to the rotation axis. The columns delineate the approximate parameter range (Reynolds, Rossby and Taylor numbers) and geometry (H, tank depth; L, particle height, D, particle width; see figure 2). † indicates the presence of a free surface. Experiments in which Taylor blocking or streamline deflections were observed are indicated.

may still produce disturbance motions with distinctive characteristics (e.g. Moore & Saffman 1969*a*).

Analytical studies of transverse particle motion may be subdivided into the low and high Taylor number limits as summarized in table 3. For $\mathscr{T} \ll 1$, Herron, Davis & Bretherton (1975) used a matched asymptotic analysis to investigate perturbations from the Stokes flow base state and so determined the hydrodynamic force on a sphere (see §3). The first effects of convective acceleration occur when $\mathscr{R}_e/\mathscr{T}^{1/2} = O(1)$. Davis & Brenner (1986) and Davis (1992) used matched asymptotic expansions to study these inertial effects in the $\mathscr{T} \ll 1$ limit.

For $\mathscr{T} \gg 1$, the flow field is determined primarily through a balance of the pressure gradient and the Coriolis acceleration (geostrophic balance), while viscous effects are confined to thin boundary layers. The geostrophic equation is solved in regions inside and outside the Taylor column and the two geostrophic solutions are then matched through viscous boundary layers along rigid boundaries and through viscous shear (Stewartson) layers separating the geostrophic regions. For $\mathscr{T} \gg 1$ Jacob (1964) investigated flow past a bounded 'fat body' and described Taylor blocking. Stewartson considered the motion of an ellipsoid in an unbounded geometry (1953) as well as a bounded geometry (1967) and also found that Taylor blocking occurs; however, in the limit where the ellipsoid approaches a disk of zero thickness, blocking disappears and there is no disturbance to the flow field. As Moore & Saffman (1969*a*) noted, "... for a body [disk] of zero thickness lying in the horizontal plane, there is no reason to anticipate the formation of a Taylor column in the usual sense, and it is impossible to get a picture of the flow field without appealing to viscous effects". They show that flow past a disk moving between two rigid boundaries exhibits no blocking, although streamlines passing over the disk are deflected through an angle. Finally, small inertial corrections were examined analytically by Ingersol (1969) and Vaziri & Boyer (1971) in studies of the flow past thin topographical disturbances.

The work described in this paper spans the low and high Taylor number limits by considering the transverse motion of a disk through an unbounded fluid undergoing solid-body rotation. Section 2 develops the dual integral equation formulation and briefly describes the necessary numerical calculations; details of the derivation are given in the Appendix. Section 3 presents results for the velocity field and hydrodynamic forces generated by the translating disk. Section 4 provides a short summary and interpretation of these results. Further details of the analytical procedures are provided in the dissertation of Tanzosh (1994).

2. Dual integral equation formulation

We construct an exact solution of the mixed boundary value problem in terms of a set of dual integral equations by first expressing the azimuthal dependence θ of the velocity and pressure fields using complex Fourier modes $e^{\pm i\theta}$ with complex-valued weighting functions. Then by using Hankel transforms to eliminate radial derivatives, a set of coupled ordinary differential equations in the axial (z) component is generated. The solutions of these constant-coefficient differential equations introduce undetermined functions of the transform variable k, which are then specified by the boundary conditions.

Researcher	$\mathscr{T}$	$\mathscr{R}_e/\mathscr{T}^{1/2}$	Geometry	Boundary	Method
Herron, *et al.* (1975)	$\ll 1$	$\ll 1$	sphere	∞	matched asymptotic expansion
Davis & Brenner (1986); Davis (1992)	$\ll 1$	$O(1)$	sphere	∞	matched asymptotic expansion
Here	any	$\ll 1$	disk	∞	dual integral equations
Stewartson (1953)	$\gg 1$	$\ll 1$	$O(1)$	∞	unsteady, geostrophic
Jacobs (1964)	$\gg 1$	$\ll 1$	$O(1)$	$O(1)$	boundary layer analysis
Stewartson (1967)	$\gg 1$	$\ll 1$	$O(1)$	$O(1)$	unsteady, geostrophic
Moore & Saffman (1969a)	$\gg 1$	$\ll 1$ †	disk	‡	boundary layer analysis
Ingersoll (1969)	$\gg 1$	$O(1)$	$O(\mathscr{R}_e/\mathscr{T})$; thin *	$O(\mathscr{T}/\mathscr{R}_e); \gg 1$	perturbation expansion
Vaziri & Boyer (1971)	$\gg 1$	$O(1)$	$O(\mathscr{T}^{-1/2})$; thin *	$O(\mathscr{T}); \gg 1$	numerical; finite difference

TABLE 3. Analytical studies related to the slow edgewise translation of a particle in a direction perpendicular to the rotation axis. GEOMETRY refers to the particle height to width or a measure of the surface disturbance height (L/D in figure 2) and BOUNDARY refers to the proximity of rigid boundaries. The ratio $\mathscr{R}_e/\mathscr{T}^{1/2}$ provides a measure of the importance of convective inertial effects in the flow. († requires $\mathscr{R}_o\,\mathscr{T}^{2/3} \ll 1$; ‡ requires $H/D \ll \mathscr{T}^{1/2}$ so that Stewartson layers remain thin and also investigates the unbounded case; *assumes that the slope of surface topology (particle) along the rotation direction is small).

2.1. *Formulation of dual integral equations*

The non-dimensional steady equations of motion, in the low Reynolds number limit and expressed relative to the rotating coordinate system, are

$$2\mathscr{T}\hat{\Omega}\wedge\boldsymbol{u} = -\nabla p + \nabla^2\boldsymbol{u} \qquad \text{and} \qquad \nabla\cdot\boldsymbol{u} = 0, \tag{2.1}$$

where p is the non-dimensional reduced pressure incorporating centrifugal and gravitational body force terms, and $\hat{\Omega}$ is a unit vector parallel to the rotation axis. Lengths have been scaled by the disk radius a, velocities by the imposed disk speed $|\boldsymbol{U}_p|$, and pressure by $\mu|\boldsymbol{U}_p|/a$. We use cylindrical coordinates (r,θ,z) centred on the disk with the z-axis parallel to Ω. The disk face $(0\leqslant r<1, z=0)$ is perpendicular to the rotation axis and translates in the x-direction with unit velocity $\boldsymbol{u}=\boldsymbol{e}_x$.

Denoting the velocity field $\boldsymbol{u}(r,\theta,z)=(u_r,u_\theta,u_z)$, the governing equations are

$$-2\mathscr{T}u_\theta = -\frac{\partial p}{\partial r} + \mathscr{L}_{-1}u_r + \frac{1}{r^2}\frac{\partial^2 u_r}{\partial\theta^2} - \frac{2}{r^2}\frac{\partial u_\theta}{\partial\theta} + \frac{\partial^2 u_r}{\partial z^2}, \tag{2.2}$$

$$2\mathscr{T}u_r = -\frac{1}{r}\frac{\partial p}{\partial\theta} + \mathscr{L}_{-1}u_\theta + \frac{1}{r^2}\frac{\partial^2 u_\theta}{\partial\theta^2} + \frac{2}{r^2}\frac{\partial u_r}{\partial\theta} + \frac{\partial^2 u_\theta}{\partial z^2}, \tag{2.3}$$

$$0 = -\frac{\partial p}{\partial z} + \mathscr{L}_0 u_z + \frac{1}{r^2}\frac{\partial^2 u_z}{\partial\theta^2} + \frac{\partial^2 u_z}{\partial z^2}, \tag{2.4}$$

$$0 = \frac{1}{r}\frac{\partial}{\partial r}(ru_r) + \frac{1}{r}\frac{\partial u_\theta}{\partial\theta} + \frac{\partial u_z}{\partial z}, \tag{2.5}$$

with the operator $\mathscr{L}_{-n}$ defined as

$$\mathscr{L}_{-n} \equiv \frac{\partial^2}{\partial r^2} + \frac{1}{r}\frac{\partial}{\partial r} - \frac{n^2}{r^2}. \tag{2.6}$$

By representing the velocity and pressure fields as functions of a complex variable, we can construct a compact solution procedure valid for arbitrary $\mathscr{T}$. Combining (2.2) $\pm$i (2.3), where $\mathrm{i}^2=-1$, results in two equations for $u_r \pm \mathrm{i}u_\theta$:

$$\mathrm{i}2\mathscr{T}(u_r+\mathrm{i}u_\theta) = -\left(\frac{\partial}{\partial r}+\frac{\mathrm{i}}{r}\frac{\partial}{\partial\theta}\right)p + \left(\mathscr{L}_{-1}+\frac{1}{r^2}\frac{\partial^2}{\partial\theta^2}+\frac{\partial^2}{\partial z^2}+\frac{2\mathrm{i}}{r^2}\frac{\partial}{\partial\theta}\right)(u_r+\mathrm{i}u_\theta), \tag{2.7}$$

$$-\mathrm{i}2\mathscr{T}(u_r-\mathrm{i}u_\theta) = -\left(\frac{\partial}{\partial r}-\frac{\mathrm{i}}{r}\frac{\partial}{\partial\theta}\right)p + \left(\mathscr{L}_{-1}+\frac{1}{r^2}\frac{\partial^2}{\partial\theta^2}+\frac{\partial^2}{\partial z^2}-\frac{2\mathrm{i}}{r^2}\frac{\partial}{\partial\theta}\right)(u_r-\mathrm{i}u_\theta). \tag{2.8}$$

Because u_r, u_θ and p are real functions, equation (2.8) is the complex conjugate of (2.7).

The trigonometric form of the imposed velocity on the disk surface, $(u_r,u_\theta,u_z)=(\cos\theta,-\sin\theta,0)$, and the linearity of the governing equations imply that the azimuthal dependence of the velocity and pressure fields away from the disk may be represented using the complex-valued Fourier modes $\mathrm{e}^{\pm\mathrm{i}\theta}$. We note that Tanzosh (1994) adopted a general Fourier mode expansion $\mathrm{e}^{\mathrm{i}n\theta}$ to analyse other disk motions. For example, the broadside translation or in-plane rotation of a disk corresponds to $n=0$; the edgewise translation or out-of-plane rotation corresponds to $n=1$. (This approach is similar to that of Happel & Brenner 1983, pp. 72–78, who use an expansion in $\sin n\theta$ and $\cos n\theta$ to describe particle motion in a Stokes flow.) Hence, we write

$$u_r+\mathrm{i}u_\theta \equiv U_{-1}(r,z)\,\mathrm{e}^{-\mathrm{i}\theta} + U_1(r,z)\,\mathrm{e}^{\mathrm{i}\theta}, \tag{2.9}$$

$$p \equiv \overline{P}(r,z)\,\mathrm{e}^{-\mathrm{i}\theta} + P(r,z)\,\mathrm{e}^{\mathrm{i}\theta}, \tag{2.10}$$

$$u_z \equiv \overline{W}(r,z)\,\mathrm{e}^{-\mathrm{i}\theta} + W(r,z)\,\mathrm{e}^{\mathrm{i}\theta}, \tag{2.11}$$

where the complex functions U_{-1}, U_1, P and W are related through the momentum and continuity equations, and an overbar represents the complex conjugate of a function. By construction, p and u_z are real functions.

Substituting the expressions (2.9)–(2.11) into the governing equations (2.4)–(2.8) and simplifying results in four equations for the four complex coefficients $U_1(r,z)$, $U_{-1}(r,z)$, $P(r,z)$ and $W(r,z)$:

$$\mathrm{i}2\mathscr{T}U_{-1} = -r^{-1}\frac{\partial}{\partial r}(r\overline{P}) + \left(\mathscr{L}_{-0} + \frac{\partial^2}{\partial z^2}\right)U_{-1}, \tag{2.12}$$

$$\mathrm{i}2\mathscr{T}U_1 = -r\frac{\partial}{\partial r}(r^{-1}P) + \left(\mathscr{L}_{-2} + \frac{\partial^2}{\partial z^2}\right)U_1, \tag{2.13}$$

$$0 = -\frac{\partial P}{\partial z} + \left(\mathscr{L}_{-1} + \frac{\partial^2}{\partial z^2}\right)W, \tag{2.14}$$

$$0 = r^{-2}\frac{\partial}{\partial r}\left(r^2 U_1\right) + \frac{\partial \overline{U}_{-1}}{\partial r} + 2\frac{\partial W}{\partial z}. \tag{2.15}$$

Hankel transforms are used to convert the partial differential equations (2.12)–(2.15) to ordinary differential equations in z. The Hankel transform $\mathscr{H}_n$ of order n and wavenumber k along with the inverse transform $\mathscr{H}_n^{-1}$ are defined by,

$$\Phi(k) = \mathscr{H}_n[\phi(r);k] \equiv \int_0^\infty r\,\phi(r)\,J_n(kr)\,\mathrm{d}r \tag{2.16}$$

$$\phi(r) = \mathscr{H}_n^{-1}[\Phi(k);r] \equiv \int_0^\infty k\,\Phi(k)\,J_n(kr)\,\mathrm{d}k. \tag{2.17}$$

We use script characters to define the appropriate Hankel transform variables:

$$\mathscr{U}_1(k,z) \equiv \mathscr{H}_2[U_1(r,z)], \tag{2.18}$$

$$\mathscr{P}(k,z), \mathscr{W}(k,z) \equiv \mathscr{H}_1[P(r,z), W(r,z)], \tag{2.19}$$

$$\overline{\mathscr{U}}_{-1}(k,z) \equiv \mathscr{H}_0[\overline{U}_{-1}(r,z)]. \tag{2.20}$$

Transforming the governing equations by taking $\mathscr{H}_0$ of the complex conjugate of (2.12), $\mathscr{H}_1$ of (2.14) and (2.15), and $\mathscr{H}_2$ of (2.13), and combining the resulting equations yields a sixth-order constant-coefficient ordinary differential equation for $\mathscr{W}$:

$$0 = (\mathscr{D}^2 + 4\mathscr{T}^2)\mathscr{W}'' - k^2\mathscr{D}^2\mathscr{W} = \mathscr{D}^3\mathscr{W} + 4\mathscr{T}^2\mathscr{W}'' \tag{2.21}$$

with the following relations for $\mathscr{U}_1$, $\overline{\mathscr{U}}_{-1}$ and $\mathscr{P}$:

$$\mathscr{P}' = \mathscr{D}\mathscr{W}, \tag{2.22}$$

$$\mathscr{U}_1 - \overline{\mathscr{U}}_{-1} = -\frac{2}{k}\mathscr{W}', \tag{2.23}$$

$$\mathrm{i}\,2\mathscr{T}(\mathscr{U}_1 + \overline{\mathscr{U}}_{-1}) = 2k\mathscr{P} + \mathscr{D}(\mathscr{U}_1 - \overline{\mathscr{U}}_{-1}), \tag{2.24}$$

where we have defined

$$()' \equiv \frac{\mathrm{d}}{\mathrm{d}z} \quad \text{and} \quad \mathscr{D} \equiv \frac{\mathrm{d}^2}{\mathrm{d}z^2} - k^2. \tag{2.25}$$

Thus the motion of a disk at arbitrary Taylor number is completely described by (i) solving (2.21) for $\mathscr{W}$, (ii) solving (2.22)–(2.24) for $\mathscr{P}$, $\mathscr{U}_1$ and $\overline{\mathscr{U}}_{-1}$, (iii) taking inverse Hankel transforms, and (iv) applying the boundary conditions to explicitly determine the unknown functions.

For this geometry, we exploit symmetry and consider only the field in the half-space $z \geqslant 0$. For $r < 1$ and $z = 0$ we enforce $\boldsymbol{u} = \boldsymbol{e}_x$ which requires

$$\overline{U}_{-1} = 1, \quad U_1 = W = 0 \qquad \text{for } r < 1,\ z = 0. \tag{2.26}$$

For $r > 1$ and $z = 0$, the velocity $\boldsymbol{u}$ and traction $\boldsymbol{e}_z \cdot \boldsymbol{T}$ from the upper half-plane $z \geqslant 0$ must match the field from the lower half-plane $z \leqslant 0$ ($\boldsymbol{T}$ denotes the stress tensor). Since the disk translates in its own plane, symmetry requires $\boldsymbol{u} \cdot \boldsymbol{e}_z = 0$ and $\boldsymbol{e}_z \cdot \boldsymbol{T} \cdot \boldsymbol{t} = 0$ along $z = 0$ for $r > 1$, where $\boldsymbol{e}_z$ is normal to the $z = 0$ plane, and $\boldsymbol{t} = \boldsymbol{e}_x$ or $\boldsymbol{e}_y$ are unit vectors tangent to this plane. These boundary conditions lead to

$$\overline{U}'_{-1} = U_1' = 0, \quad W = 0 \qquad \text{for } r > 1,\ z = 0. \tag{2.27}$$

Assuming the fields decay as $z \to \infty$, the solution of (2.21), in the half-space $z \geqslant 0$, introduces three complex-valued functions $A_1(k)$, $A_2(k)$ and $A_3(k)$. These functions are determined through the boundary conditions in the plane of the disk. After taking the appropriate inverse Hankel transforms we arrive back at the complex-valued physical space variables, U_{-1}, U_1, W and P:

$$W(r,z) = \int_0^\infty \sum_{j=1}^{3} kA_j(k)\, \mathrm{e}^{-S_j z}\, J_1(kr)\, \mathrm{d}k, \tag{2.28}$$

$$P(r,z) = -\int_0^\infty \sum_{j=1}^{3} k\frac{(S_j^2 - k^2)}{S_j} A_j(k)\, \mathrm{e}^{-S_j z}\, J_1(kr)\, \mathrm{d}k, \tag{2.29}$$

$$U_1(r,z) = \int_0^\infty \sum_{j=1}^{3} \frac{S_j(S_j^2 - k^2 + \mathrm{i}2\mathscr{T})}{S_j^2 - k^2} A_j(k)\ \mathrm{e}^{-S_j z}\, J_2(kr)\, \mathrm{d}k, \tag{2.30}$$

$$U_{-1}(r,z) = -\int_0^\infty \sum_{j=1}^{3} \frac{\overline{S}_j(\overline{S}_j^2 - k^2 + \mathrm{i}2\mathscr{T})}{\overline{S}_j^2 - k^2} \overline{A}_j(k)\, \mathrm{e}^{-\overline{S}_j z}\, J_0(kr)\, \mathrm{d}k, \tag{2.31}$$

where $\pm S_j$ ($j = 1, 2, 3$) are the six roots of the polynomial

$$(S_j^2 - k^2)^3 + 4\mathscr{T}^2 S_j^2 = 0 \qquad \text{with} \qquad \mathrm{Re}(S_j) \geqslant 0. \tag{2.32}$$

The characteristic equation (2.32) admits one pair of real roots, labelled $\pm S_1$, and two pairs of complex-conjugate roots $\pm S_2$ and $\pm S_3 = \pm\overline{S}_2$. The roots are labelled to ensure that the fields (2.28)–(2.31) decay at infinity.

Along $z = 0$, the boundary condition is $W = 0$ for all r and implies that $A_1 = -(A_2 + A_3)$. It is convenient to introduce two new unknown functions Ψ_1 and Ψ_2 which are linear combinations of A_2 and A_3, and chosen so that the boundary conditions for $r > 1$ have a simple form given by (2.34) below. The details of this rearrangement are described in the Appendix.

The boundary conditions on $z = 0$ for U_{-1} and U_1 result in coupled dual integral equations for the complex-valued unknown functions Ψ_1 and Ψ_2 which satisfy

$$\left.\begin{aligned} \overline{U}_{-1}(r,0): \quad -1 &= \int_0^\infty \left[c_{11}(k,0)\,\Psi_1(k) + c_{12}(k,0)\,\Psi_2(k) \right] J_0(kr)\,\mathrm{d}k \\ U_1(r,0): \quad 0 &= \int_0^\infty \left[c_{21}(k,0)\,\Psi_1(k) + c_{22}(k,0)\,\Psi_2(k) \right] J_2(kr)\,\mathrm{d}k \end{aligned}\right\} \text{for } r < 1, \tag{2.33}$$

and

$$\left.\begin{aligned} \overline{U}'_{-1}(r,0): \quad 0 &= \int_0^\infty \Psi_1(k)\,J_0(kr)\,\mathrm{d}k, \\ U'_1(r,0): \quad 0 &= \int_0^\infty \Psi_2(k)\,J_2(kr)\,\mathrm{d}k, \end{aligned}\right\} \text{for } r > 1, \tag{2.34}$$

where the coupling coefficients $c_{ij}(k,z)$ are known functions that are given in the Appendix. The solution of the integral equations in terms of Ψ_1 and Ψ_2 then directly follows from a solution procedure outlined by Sneddon (1966, pp. 129). Finally given Ψ_1 and Ψ_2, the velocity and pressure fields are found using the analytic expressions (2.9)–(2.11) and (2.28)–(2.31).

2.2. *Solution of the dual integral equations*

Tranter (1966) and Sneddon (1966) show how to reduce dual integral equations with Bessel function kernels to a system of algebraic equations by representing the unknown functions as infinite series of Bessel functions and then imposing an orthogonality condition to develop algebraic equations. An alternative procedure for treating the system of dual integral equations is described by Davis (1991,1993). Here, following Sneddon's analysis, we represent the functions $\{\Psi_i\}$ using an expansion in Bessel functions having constant complex-valued weights a_{1m} and a_{2m}:

$$\Psi_1(k) = k^{1-\beta} \sum_{m=0}^{\infty} a_{1m} J_{2m+\beta}(k), \tag{2.35}$$

$$\Psi_2(k) = k^{1-\beta} \sum_{m=0}^{\infty} a_{2m} J_{2m+2+\beta}(k). \tag{2.36}$$

By construction, these expansions satisfy (2.34) for $r > 1$. β is a parameter which can be chosen to facilitate convergence of integrals and is discussed below. Tranter's method is completed in four steps: (i) substitute the expansions for $\{\Psi_i(k)\}$ into (2.33); (ii) multiply by $r^{\nu+1}(1-r^2)^{\beta-1}\mathscr{P}_n(\beta+\nu,\nu+1;r^2)$ where $\mathscr{P}_n$ is a Jacobi polynomial and $\nu = 0$ is used for the equation with J_0 and $\nu = 2$ is used with J_2; (iii) integrate the equations from $r = 0 \to 1$; (iv) use the identities (e.g. Magnus, Oberhettinger & Soni 1966)

$$k^{-\beta} J_{2n+\nu+\beta}(k) = \frac{\Gamma(\nu+n+1)}{2^{\beta-1}\,\Gamma(\nu+1)\,\Gamma(n+\beta)} \int_0^1 r^{\nu+1}(1-r^2)^{\beta-1}\mathscr{P}_n(\beta+\nu,\nu+1;r^2)\,J_\nu(kr)\,\mathrm{d}r \tag{2.37}$$

and

$$\int_0^1 r^{2\nu+1}(1-r^2)^{\beta-1}\,\mathscr{P}_n(\beta+\nu,\nu+1;r^2)\,\mathrm{d}r = \frac{\Gamma(\nu+1)\Gamma(\beta)}{2\Gamma(\nu+\beta+1)}\,\delta_{0n}. \tag{2.38}$$

These steps reduce the integral equations to an infinite set of complex-valued algebraic equations relating the coefficients $\{a_{1m}, a_{2m}\}$:

$$-\frac{1}{2^{\beta}\beta\Gamma(\beta)}\begin{Bmatrix}\delta_{0n}\\ 0\end{Bmatrix}=\sum_{m=0}^{\infty}\begin{bmatrix}\Phi_{11}(n,m) & \Phi_{12}(n,m+1)\\ \Phi_{21}(n+1,m) & \Phi_{22}(n+1,m+1)\end{bmatrix}\begin{Bmatrix}a_{1m}\\ a_{2m}\end{Bmatrix} \tag{2.39}$$

for $n = 0, 1, 2\cdots$, where $\Gamma(\beta)$ is the Gamma function and where $\Phi_{ij}(n,m)$ denotes the nm-component of a second rank submatrix:

$$\Phi_{ij}(n,m) \equiv \int_0^{\infty} k^{1-2\beta}\, c_{ij}(k, z=0)\, J_{2m+\beta}(k)\, J_{2n+\beta}(k)\, \mathrm{d}k. \tag{2.40}$$

The hydrodynamic force $\boldsymbol{F} = (F_x, F_y, F_z)$ and torque $\boldsymbol{L} = (L_x, L_y, L_z)$ acting on the disk are calculated by integrating the surface tractions. The azimuthal integration is straightforward to evaluate using expressions (2.9)–(2.11) for $\boldsymbol{u}$ and p and leads to

$$F_x + \mathrm{i}F_y = 2\pi \int_0^1 r\, U'_{-1}\Big|_{0^-}^{0^+} \mathrm{d}r, \qquad F_z = 0, \tag{2.41}$$

and

$$L_x - \mathrm{i}L_y = 2\pi\mathrm{i} \int_0^1 r^2\big(-P + 2W'\big)\Big|_{0^-}^{0^+} \mathrm{d}r, \qquad L_z = 0. \tag{2.42}$$

Substituting the Bessel function expansions (2.35)–(2.36) into the expression for the force (2.41) and evaluating the integral, we find that only the first term yields a non-zero contribution. The hydrodynamic force is thus given by

$$F_x + \mathrm{i}\,F_y = \frac{4\pi}{2^{\beta}\beta\Gamma(\beta)}\, a_{10} \qquad \text{and} \qquad L_x - \mathrm{i}L_y = 0. \tag{2.43}$$

This result uses $U'_{-1}\big|_{0^-}^{0^+} = 2U_{-1}(r, z=0)$ and $\big(-P + 2W'\big)\big|_{0^-}^{0^+} = 0$.

The numerical solution of the linear system represented by equations (2.39) and (2.40) is straightforward. The integrals $\Phi_{ij}(n,m)$ forming the elements of the matrix involve products of Bessel functions. An efficient quadrature scheme for integrands involving products of Bessel functions was developed by Lucas (1995) and is used to evaluate these integrals to a prescribed accuracy (typically with absolute and relative errors less than 10^{-9}). The linear system is solved using a standard IMSL routine (DLSACG) to determine the expansion weights $\{a_{1m}, a_{2m}\}$.

The value of β affects the number of terms required in the expansions (2.35)–(2.36) to achieve a prescribed accuracy. As noted by Vedensky & Ungarish (1994) and Ungarish & Vadensky (1995), the 'correct' β is that value which captures the behaviour of the stress singularity near the disk edge. Based on the $\mathscr{T} = 0$ analysis, one would thus take $\beta = 1/2$. We see this fact borne out in table 4, in which values of the velocity field at a point $(r, \theta, z) = (0.5, 0, 0)$ on the disk surface and the hydrodynamic force are calculated using (2.35)–(2.36) and compared for various values of β. The actual velocity at this point is $(u_r, u_\theta) = (1, 0)$. Table 5 demonstrates the effects of the expansion truncation on the hydrodynamic force. Keeping $N = 15$ terms in the expansions ensures less than a 0.1% error in the hydrodynamic force, even when the less than optimal value of $\beta = 1.0$ is taken. The numerical results in §3 use $N = 15$ and $\beta = 1.0$.

β	u_r	Drag	Lift
1.0	0.997 615	13.991 54	−12.491 87
0.75	0.999 423	13.997 79	−12.500 63
0.625	0.999 685	14.000 27	−12.502 86
0.5	1.000 000	14.000 11	−12.503 62

TABLE 4. The effect the parameter β (equation (2.36)) has on the calculated velocity and hydrodynamic force. The Taylor number $\mathscr{T} = 500$ and the truncation order $N = 15$. The velocity is evaluated at a point on the disk surface $(r, \theta, z) = (0.5, 0, 0)$ and can be compared to the actual value $u_r = 1$.

	$\mathscr{T} = 1$		$\mathscr{T} = 500$		$\mathscr{T} = 10^4$	
N	Drag	Lift	Drag	Lift	Drag	Lift
5	1.448	−0.3908	13.914	−12.444	59.520	−57.909
10	1.452	−0.3925	13.974	−12.480	59.642	−57.905
15	1.453	−0.3929	13.991	−12.491	59.700	−57.932
20	1.453	−0.3931	13.993	−12.496	59.723	−57.949
25	1.453	−0.3932	13.999	−12.499	59.734	−57.958

TABLE 5. Convergence of the non-dimensional hydrodynamic force (drag and lift) for $\mathscr{T} = 1$, 500 and 10^4 as a function of the truncation order N; $\beta = 1.0$.

3. Results

This section discusses the force and velocity fields associated with the transverse translation of a disk edgewise through an unbounded rotating fluid. We first describe the hydrodynamic force as a function of the Taylor number and then examine in detail the velocity field with particular attention given to the limit $\mathscr{T} \gg 1$.

For small Taylor numbers $\mathscr{T} \ll 1$, the fluid motion appears qualitatively to be a Stokes flow with a superimposed swirl. For large Taylor numbers, $\mathscr{T} \gg 1$, the flow features a thin Ekman boundary layer adjacent to the disk and a weak secondary flow outside the Ekman layer (observed from a reference frame in which the disk is stationary). The secondary flows consist of two counter-rotating eddies aligned parallel to the rotation axis and extending into the far field. The velocity magnitudes away from the immediate vicinity of the disk are small, typically 1–2% of the disk speed when $\mathscr{T} = 500$. The Taylor blocking phenomenon does not occur; that is, a column of fluid does not move with the translating disk, although the presence of background rotation is nevertheless evident.

3.1. *Ekman layer near a rigid planar wall*

It is useful to first consider the disturbance flow, governed by the linearized rotating equations, created by a translating rigid plate of infinite extent aligned perpendicular to the rotation axis. This model problem captures many of the features of disk motion at high Taylor numbers and is a classical problem in rotating fluid dynamics which is analysed, for example, in Batchelor (1967, §4.4). The plate is located in the $z = 0$ plane, perpendicular to the rotation axis, and the fluid extends into the region $z > 0$. It is common to assume that far away from the plate, a constant pressure gradient along the y-direction creates a uniform, unidirectional flow in the x-direction as prescribed by the geostrophic equation. However, here it is more appropriate to suppose that the plate translates in the x-direction with speed U and the far-field fluid is quiescent. Near the plate, the magnitude of the Coriolis force is comparable to

the viscous force, velocity field variations occur within an Ekman layer of thickness $\delta = (\nu/\Omega)^{1/2}$ adjoining the plate, and the velocity field is

$$(u_x, u_y, u_z) = U\,\mathrm{e}^{-z/\delta}\left(\cos\frac{z}{\delta}, -\sin\frac{z}{\delta}, 0\right). \tag{3.1}$$

The boundary layer thickness, which may be defined as the height where the velocity field falls to 1% of the imposed plate speed U, is located at $z_{BL}/\delta \approx 4.1$. The viscous stresses tangent to the plate surface ($z = 0$) created by this flow are given by

$$\mu\left.\frac{\partial u_x}{\partial z}\right|_{z=0} \boldsymbol{e}_x + \mu\left.\frac{\partial u_y}{\partial z}\right|_{z=0} \boldsymbol{e}_y = -\frac{\mu U}{\delta}(\boldsymbol{e}_x + \boldsymbol{e}_y). \tag{3.2}$$

Hence the hydrodynamic force, which resists motion of the plate, is directed at an angle of 135° measured clockwise from the translation direction. The net volume flux, per unit width, in the Ekman layer is

$$\int_0^\infty (u_x\,\boldsymbol{e}_x + u_y\,\boldsymbol{e}_y)\,\mathrm{d}z = \frac{\delta U}{\sqrt{2}}(\boldsymbol{e}_x - \boldsymbol{e}_y). \tag{3.3}$$

Thus there is a net volume flux directed 45° clockwise to the direction in which the plate is translating.

We use these results for a translating infinite plate to interpret the velocity field and traction created by the edgewise translation of a disk at high Taylor numbers. For a disk of radius a, a boundary layer of thickness $\delta/a = O(\mathscr{T}^{-1/2})$ develops. In terms of this boundary layer length scale, the disk centre is far from the disk edge and we anticipate that the flow features near the disk centre are similar to those above an unbounded plate. The drag and lift on the disk are estimated by taking the stress distribution on the disk to be the viscous stresses of the infinite-plate solution, which may integrated over the disk surface to obtain the dimensional hydrodynamic force $\boldsymbol{F}$:

$$\boldsymbol{F} = -2\pi\mu U a \mathscr{T}^{1/2}(\boldsymbol{e}_x + \boldsymbol{e}_y). \tag{3.4}$$

Thus the viscous force resisting translation of the disk is proportional to $\mathscr{T}^{1/2}$ and acts in a direction 135° measured clockwise from the translation direction.

3.2. *Hydrodynamic forces*

The hydrodynamic force on the disk may be resolved into components anti-parallel to the translation direction (drag) and perpendicular to the translation and rotation axes (lift). In the problem studied here, the disk translates in the x-direction through a fluid in solid-body rotation about the z-axis, and creates a drag force in the negative x-direction and a lift in the negative y-direction. Equation (3.4) describing the high Taylor number limit demonstrates this response. At zero Taylor number, the dimensional drag reduces to the Stokes drag on a disk $32U\mu a/3$ and the lift is identically zero.

Figure 3 shows the numerically determined hydrodynamic force (drag and lift), non-dimensionalised with respect to the Stokes drag, over a range of Taylor numbers $10^{-1} \leqslant \mathscr{T} \leqslant 10^5$. The solid curve displays the drag and the dashed curve displays the lift. The numerical solution indicates that the drag and lift scale as $\mathscr{T}^{1/2}$ for large Taylor numbers, a scaling which is consistent with the viscous stresses created in the Ekman layer adjoining an infinite plate. At small Taylor numbers, the non-dimensional drag approaches one, and the lift approaches zero.

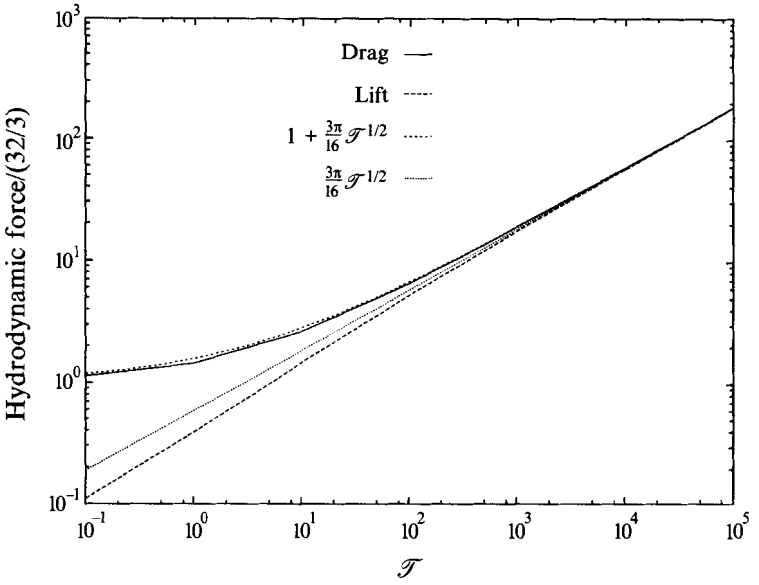

FIGURE 3. The dimensionless hydrodynamic force on a disk translating perpendicular to the rotation axis. The drag is in the opposite direction of the imposed velocity; the lift is perpendicular to the velocity/rotation directions. Also shown are the estimates for the drag and lift that are given by equation (3.5).

A simple formula for the drag and lift, valid for *all* Taylor numbers, combines the high Taylor number estimates given by (3.4) and the Stokes flow result to yield the non-dimensional estimates for the drag F_x and lift F_y,

$$\frac{F_x}{32/3} = -\left(1 + \frac{3\pi}{16}\mathscr{T}^{1/2}\right) \quad \text{and} \quad \frac{F_y}{32/3} = -\frac{3\pi}{16}\mathscr{T}^{1/2}, \tag{3.5}$$

which are also presented in figure 3. These simple formulae are within 10% of the numerically determined values of the drag F_x for all $\mathscr{T}$ and the lift F_y for $\mathscr{T} > 100$. Moreover, the formulae become more accurate at higher Taylor numbers: the drag result (3.5) is accurate to within 1% for $\mathscr{T} > 1000$, and the lift to within 1% for $\mathscr{T} > 50000$.

We are thus led to propose an estimate for the hydrodynamic force created by a disk undergoing *arbitrary* translational motion $\boldsymbol{U}$, provided the disk face remains perpendicular to the rotation axis. Using the results presented in Tanzosh & Stone (1994, equation 4.3; see also Vedensky & Ungarish 1994) for the drag on an axisymmetric disk translating parallel to the rotation axis, and equation (3.5) given above, the non-dimensional hydrodynamic force $\boldsymbol{F} = (F_x, F_y, F_z)$ can be estimated for *any* Taylor number using

$$\frac{\boldsymbol{F}}{32/3} = -\begin{bmatrix} 1 + \frac{3\pi}{16}\mathscr{T}^{1/2} & -\frac{3\pi}{16}\mathscr{T}^{1/2} & 0 \\ \frac{3\pi}{16}\mathscr{T}^{1/2} & 1 + \frac{3\pi}{16}\mathscr{T}^{1/2} & 0 \\ 0 & 0 & \frac{3}{2}\left(1 + \frac{32}{21\pi}\mathscr{T}^{1/2} + \frac{1}{3}\mathscr{T}\right) \end{bmatrix} \cdot \boldsymbol{U}. \tag{3.6}$$

The accuracy of this equation for in-plane motion is described above. For broadside motion, this estimate is within 7% of the numerically determined exact results presented by Vedensky & Ungarish (1994). These hydrodynamic force estimates provide an upper bound for the numerically determined results.

The high Taylor number scalings for the drag and lift on a disk translating edgewise along a plane perpendicular to the rotation axis are a consequence of viscous boundary layers of thickness $O(\mathscr{T}^{-1/2})$ generating viscous forces $O(\mathscr{T}^{1/2})$. In contrast, the drag on a disk translating broadside scales as $\mathscr{T}$ in the high Taylor number limit since the dominant resistance arises from the $O(\mathscr{T})$ geostrophic pressure difference fore and aft of the particle.

The disk (of zero thickness) translating edgewise does not create the usual Taylor column, as we illustrate in §§3.3–3.5, and would be expected to have a smaller drag than a comparable body of a finite thickness, which creates a Taylor column. For comparison, we provide the low and high Taylor number asymptotic estimates for the hydrodynamic force on a translating sphere. The low Taylor number approximation (Herron *et al.* 1975; Childress 1964) is

$$\frac{\boldsymbol{F}}{6\pi} = -\begin{bmatrix} 1+\frac{5}{7}\mathscr{T}^{1/2} & -\frac{3}{5}\mathscr{T}^{1/2} & 0 \\ \frac{3}{5}\mathscr{T}^{1/2} & 1+\frac{5}{7}\mathscr{T}^{1/2} & 0 \\ 0 & 0 & 1+\frac{4}{7}\mathscr{T}^{1/2} \end{bmatrix} \cdot \boldsymbol{U} + O(\mathscr{T}) \quad \text{for } \mathscr{T} \ll 1 \tag{3.7}$$

and the high Taylor number approximation (Stewartson 1953) is

$$\frac{\boldsymbol{F}}{6\pi} = -\mathscr{T}\begin{bmatrix} \frac{16\pi}{9(16+\pi^2)} & -\frac{4\pi^2}{9(16+\pi^2)} & 0 \\ \frac{4\pi^2}{9(16+\pi^2)} & \frac{16\pi}{9(16+\pi^2)} & 0 \\ 0 & 0 & \frac{8}{9\pi} \end{bmatrix} \cdot \boldsymbol{U} \quad \text{for } \mathscr{T} \gg 1. \tag{3.8}$$

The high Taylor number estimates of the non-dimensional drag on a disk and sphere translating parallel to the rotation axis are identical and are attributable to the geostrophic pressure differences fore and aft of the particle. The shape of the particle is unimportant since the equatorial radius determines the dominant contribution to the drag. However, the shape is important when the particle translates perpendicular to the rotation axis. For a disk of zero thickness, the hydrodynamic force scales as $\mathscr{T}^{1/2}$ owing to viscous stresses, whereas for the sphere, the forces scale as $\mathscr{T}$ which appears to be related to the formation of a Taylor column accompanying the particle. It is tempting to combine (3.7) and (3.8) in a manner similar to (3.6), but we currently lack experimental or numerical evidence for justifying such a claim. We are attempting to verify this conjecture by using the boundary integral method developed by Tanzosh & Stone (1994) to investigate the transverse translation of a rigid sphere.

3.3. *Velocity in the plane of the disk*

Figure 4 shows the two components of the velocity field in the plane of the translating disk ($z = 0$) as a function of position r along the direction of motion ($\theta = 0$). As the Taylor number approaches zero, the velocity field approaches the

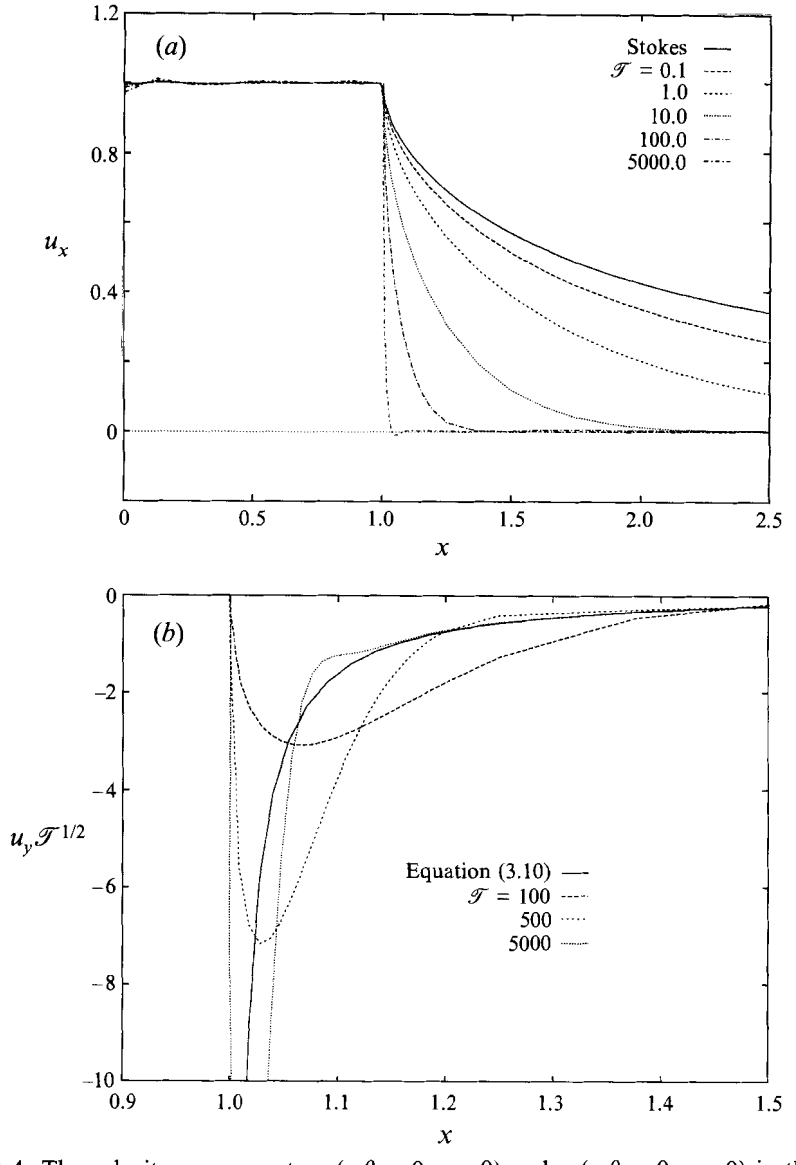

FIGURE 4. The velocity components $u_x(r, \theta = 0, z = 0)$ and $u_y(r, \theta = 0, z = 0)$ in the plane of the disk along the direction of translation. The disk occupies the region $r < 1$ and translates with unit velocity $(u_x, u_y) = (1, 0)$. As $\mathscr{T} \to 0$, the velocity approaches the Stokes flow result given by equation (3.9). For $\mathscr{T} \to \infty$, the velocity component u_x rapidly decays outside the disk edge; the component u_y develops a spiked structure with magnitude scaling as $u_y/\mathscr{T}^{-1/2}$, which agrees with the asymptotic result of Moore & Saffman, equation (3.10), shown by the solid curve.

Stokes flow result

$$u_x(r, \theta = 0, z = 0) = \frac{2}{\pi}\left[\frac{(r^2-1)^{1/2}}{3r^2} + \sin^{-1}\left(\frac{1}{r}\right)\right],$$
$$u_y(r, \theta = 0, z = 0) = 0 \qquad (\mathscr{T} = 0). \tag{3.9}$$

As the Taylor number increases, the gradient of the velocity field changes rapidly in the vicinity of the disk edge. The component u_x approaches a step function, with

only a minimal flow disturbance exterior to the disk edge. This feature is consistent with the geostrophic flow limit for which large velocity gradients occur in narrow viscous shear layers. Also, with increasing Taylor number, the component u_y develops a narrow spiked structure over the edge of the disk. Moore & Saffman's (1969*a*) analysis of a disk translating through an unbounded fluid when $\mathscr{T} \gg 1$ also suggests a similar spike-like flow structure. For example, Moore & Saffman's equation (6.7) describing the velocity component u_y in the $z = 0$ plane can be shown to reduce to

$$u_y(r, \theta = 0, z = 0) \approx \frac{1}{4\mathscr{T}^{1/2}} \int_0^\infty k J_1(k) \Big[J_0(kr) - J_2(kr) \Big] \, \mathrm{d}k \quad \text{for} \quad \mathscr{T} \to \infty. \tag{3.10}$$

The numerical evaluation of this result is included in figure 4(*b*) which plots the scaled velocity $u_y \mathscr{T}^{1/2}$ versus position r for various Taylor numbers. The velocity fields determined here are in good agreement with this asymptotic result of Moore & Saffman, though, as a referee indicated, Moore & Saffman's result is singular as $r \to 1^+$ since in their analysis an $O(\mathscr{T}^{-1/2} \times \mathscr{T}^{-1/2})$ region at the disk edge is replaced by a singularity.

The slight wobbles in the velocity field along the disk surface ($r < 1$) result from truncating the Bessel function expansions in §2. Increasing the order of the expansion decreases this numerical error and, in general, calculating the velocity to a given accuracy near the disk surface requires more terms than for a position far from the disk.

3.4. *Velocity on the centreline ($\mathscr{T} \gg 1$)*

Figures 5 and 6 present the velocity components, u_x and u_y, calculated at axial z-positions along the centreline ($r = 0$), for four values of the Taylor number between $100 \leqslant \mathscr{T} \leqslant 5000$; the axial velocity component u_z is identically zero along $r = 0$ based on the symmetry of the flow field. Different characteristics of the velocity field inside/outside the Ekman layer become apparent by introducing two distinct length scales. Recall that the boundary layer thickness $z_{BL} \approx 4\mathscr{T}^{-1/2}$ was previously defined as the height where the velocity falls to 1% of the boundary speed.

Outside the Ekman layer ($z > 4\mathscr{T}^{-1/2}$), the axial distance z is scaled by $\mathscr{T}$ and the magnitude of the velocities by $\mathscr{T}^{-1/2}$ (see figure 5). This scaling, which is consistent with a weak viscous decay of the disturbance flow fields in rotating unbounded flows (Moore & Saffman 1969*a*), succeeds in collapsing the velocity profiles. The magnitudes of the two velocity components are approximately the same $|u_y| \approx |u_x| = O(\mathscr{T}^{-1/2})$. We observe that both velocity components undergo slight increases in magnitude with increasing distance from the edge of the Ekman layer, reaching a maximum at a scaled distance $z/\mathscr{T} \approx 0.04$–$0.05$. For larger distances, the velocity magnitudes decay monotonically.

The results described above are consistent with Moore & Saffman's (1969*a*) boundary layer analysis, valid in the limit $\mathscr{T} \gg 1$, of the edgewise motion of a disk through an unbounded fluid. Their solution for the u_x and u_y velocity components has the form

$$u_x(r = 0, z) = u_y(r = 0, z) = \frac{1}{4\mathscr{T}^{1/2}} \int_0^\infty k \, \mathrm{e}^{-\frac{1}{2}k^3|z|/\mathscr{T}} J_1(k) \, \mathrm{d}k \tag{3.11}$$

along the centreline $(x, y) = (0, 0)$ when $\mathscr{T} \gg 1$. The numerical evaluation of this expression is included in figure 5 and is in good agreement with the analysis presented here for arbitrary $\mathscr{T}$.

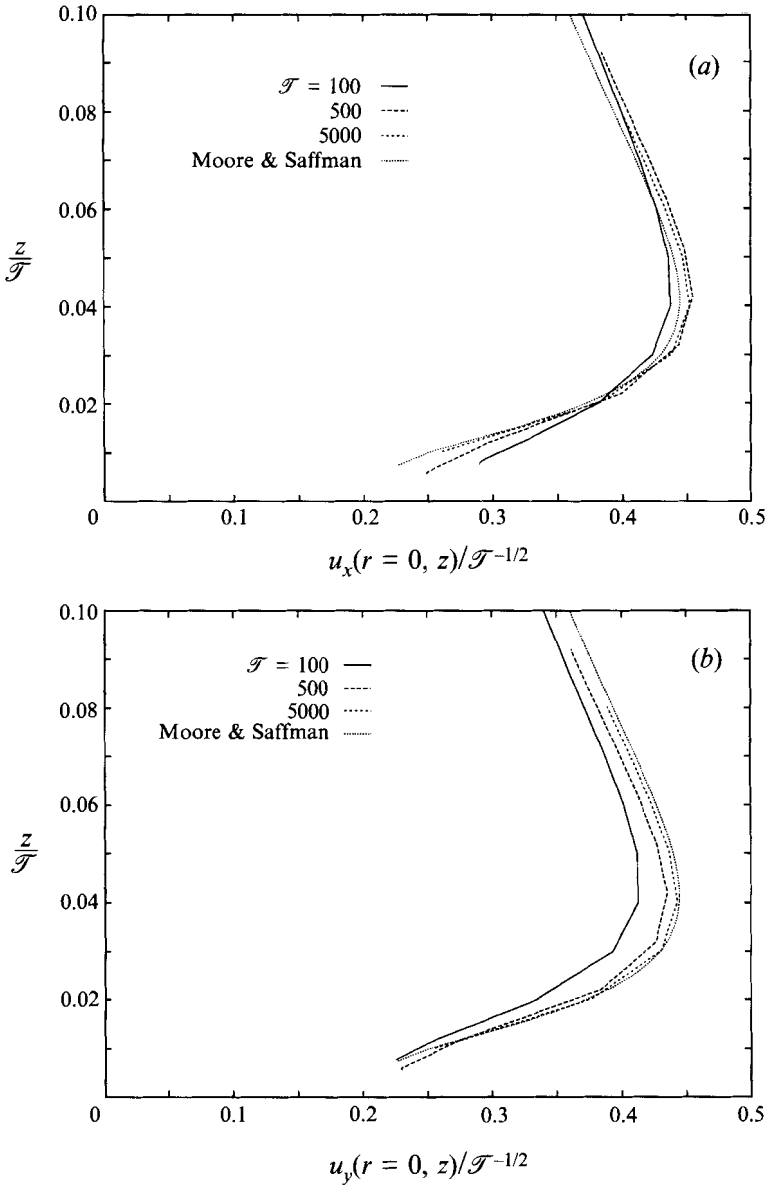

FIGURE 5. The velocity field $u_x(r = 0, z/\mathscr{T})$ and $u_y(r = 0, z/\mathscr{T})$ in the region *outside* the Ekman layer. The magnitude of the velocity is scaled by $\mathscr{T}^{-1/2}$; the distance from the disk surface is scaled by $\mathscr{T}$. The results, which collapse to a single curve in the high Taylor number limit, are in agreement with the asymptotic results of Moore & Saffman (1969*a*) given by (3.11). Note that these scalings are inappropriate in the Ekman layer near $z = 0$.

Within the Ekman layer, the axial scaling $z/\mathscr{T}^{-1/2}$ collapses results for different Taylor numbers (figure 6). For sufficiently large Taylor numbers, the Ekman layer thickness is small compared with the disk radius $\delta/a = O(\mathscr{T}^{-1/2}) \ll 1$. Hence the influence of the disk edge is expected to be small near the disk centre and the fluid motion should be similar to that along an infinite plate, equation (3.1). Figure 6 shows quantitative agreement between the analytical result for the infinite plate and the centreline velocity of the finite disk. Only toward the outer edge of the Ekman

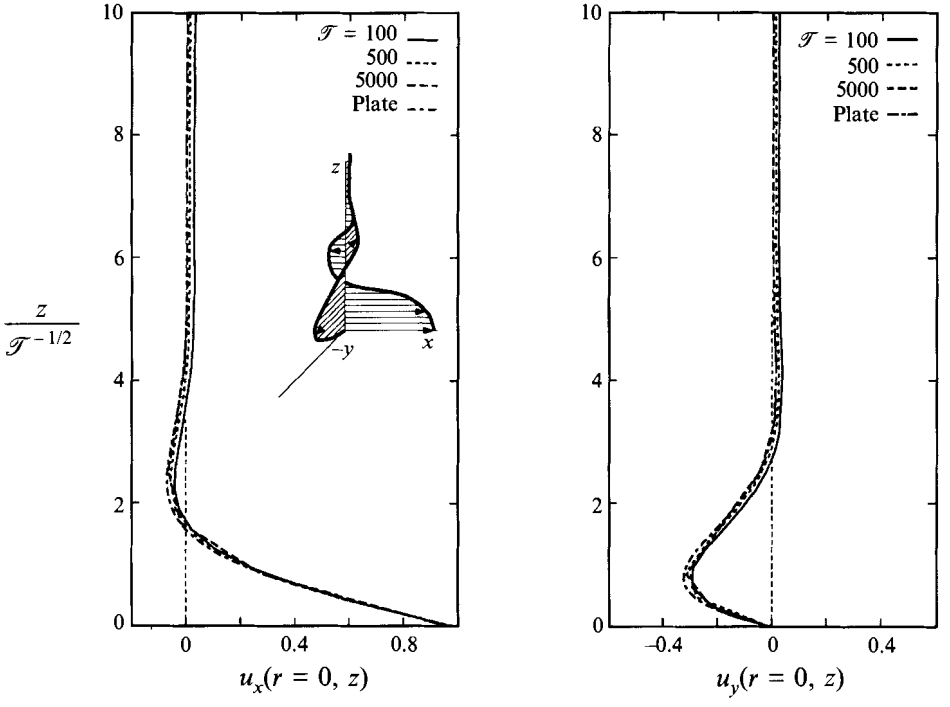

FIGURE 6. The velocity field $u_x(r = 0, z/\mathscr{T}^{-1/2})$ and $u_y(r = 0, z/\mathscr{T}^{-1/2})$ for positions along the centerline *inside* the Ekman layer adjacent to the disk surface. The distance from the disk surface is scaled by the Ekman layer thickness $\mathscr{T}^{-1/2}$. Also shown is the velocity field corresponding to a translating plate as given by equation (3.1).

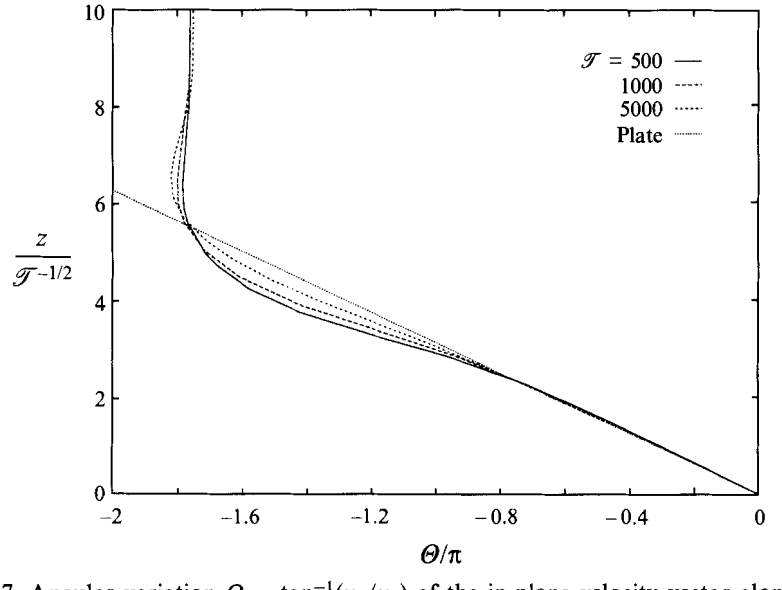

FIGURE 7. Angular variation $\Theta = \tan^{-1}(u_y/u_x)$ of the in-plane velocity vector along the centreline within the Ekman layer. The height above the disk z is scaled by the Ekman length $\mathscr{T}^{-1/2}$. Also shown is the angular dependence of the in-plane velocity vector for an infinite plate based on the velocity fields given in equation (3.1). (The $\mathscr{T} = 5000$ calculation uses $N = 25$.)

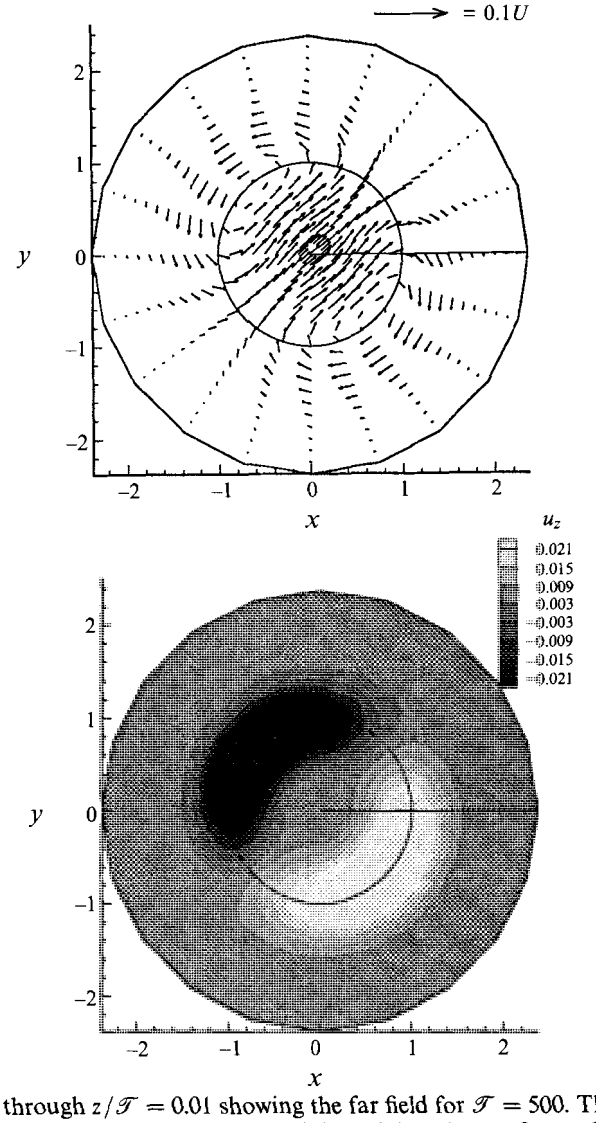

FIGURE 8. Plan view through $z/\mathscr{T} = 0.01$ showing the far field for $\mathscr{T} = 500$. The unit disk is centred at the origin and translates along the x-axis from left to right. The top figure shows the velocity field in the plane; the bottom figure is a contour plot of the axial velocity field. Two counter-rotating eddies centred over the edge of the disk create a net flow directed at an angle $\theta = -45°$ and 135° from the translation direction. The eddies are regions of the largest axial flow observed outside the Ekman layer (see figures 9 and 10).

layer do the two results diverge: whereas the velocity field of an infinite plate continues to decay exponentially fast with increasing distance from the plate, the velocity field for the translating disk has magnitude $u_x \approx u_y = O(\mathscr{T}^{-1/2})$ which couples to the outer region (figure 5).

The in-plane velocity vectors (u_x, u_y) along the centreline rotate through nearly a full revolution with increasing height above the disk and have a spiralling structure referred to as an Ekman spiral. We define the angular dependence Θ of the in-plane velocity vector, measured from the x-axis, according to

$$\tan\Theta = \frac{u_y}{u_x}. \tag{3.12}$$

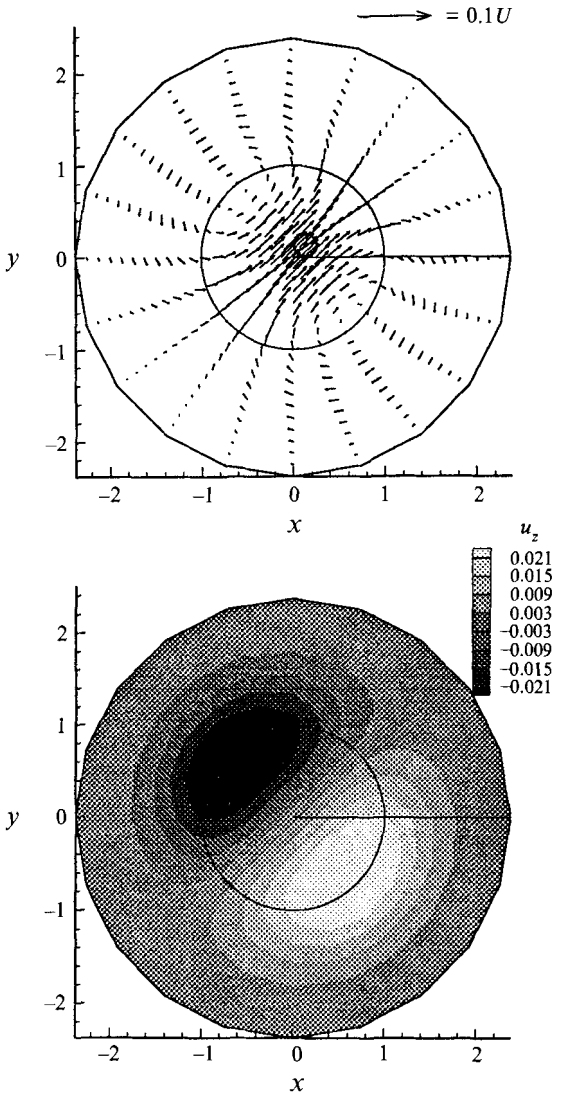

FIGURE 9. Plan view showing the far field at a section through $z/\mathscr{T} = 0.05$ for $\mathscr{T} = 500$ (see figure 8).

For an infinite plate (3.1), the angular dependence varies linearly with distance, $\Theta \propto -z$. Figure 7 shows the calculated angular dependence Θ as a function of the distance from the disk $z/\mathscr{T}^{-1/2}$. Within the Ekman layer the angular dependence of the disk closely follows that of the infinite plate. Outside the Ekman layer, the direction of the in-plane velocity vector approaches an asymptotic value $\Theta = 45°$ from the x-axis. This result is related to the finite dimension of the disk creating secondary flows which are studied in detail in the next section.

3.5. *Plan view of the velocity ($\mathscr{T} \gg 1$)*

In order to illustrate the three-dimensional nature of the flow field, we show in figures 8–14 the in-plane velocity components u_x and u_y in horizontal sections of the flow, and contour plots showing the axial velocity u_z. The views are looking down on the disk at planes z = constant, so that the unit disk ($r < 1$) is centred at the

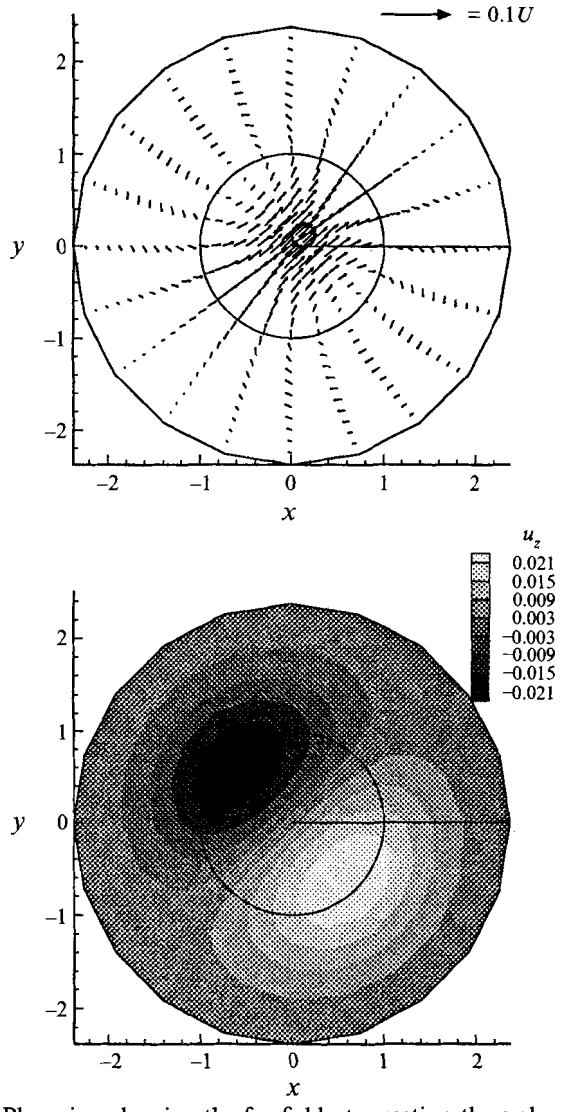

FIGURE 10. Plan view showing the far field at a section through $z/\mathscr{T} = 0.075$ for $\mathscr{T} = 500$ (see figure 8).

origin and is translating to the right with unit velocity. The x-axis is indicated by the solid horizontal line; the angle θ is measured from the x-axis in the counter-clockwise sense. The contour plots of the axial velocity use dark shades to indicate negative velocity (down-flow) and light shades to indicated positive velocity (up-flow).

Figures 8–10 illustrate fluid motion outside the Ekman layers at axial distances $z = 5, 25, 37.5$ for $\mathscr{T} = 500$ or scaled distances $z/\mathscr{T} = 0.01$, 0.05, 0.75, respectively. Over large portions of the disk, the flow is uniformly directed at an angle $\theta = 45°$ from the leading edge (x-axis). This flow is created by two counter-rotating eddies, centred over the edge of the disk at angles $\theta = -45°$ and 135° from the x-axis. These eddies are regions of relatively large axial flow that move upward near the leading edge and downward at the trailing edge. This columnar structure extends from the Ekman layer into the far field with only a gradual viscous decay (previously quantified in figure 5) and broadening of the eddies. For $\mathscr{T} = 500$, the axial velocity

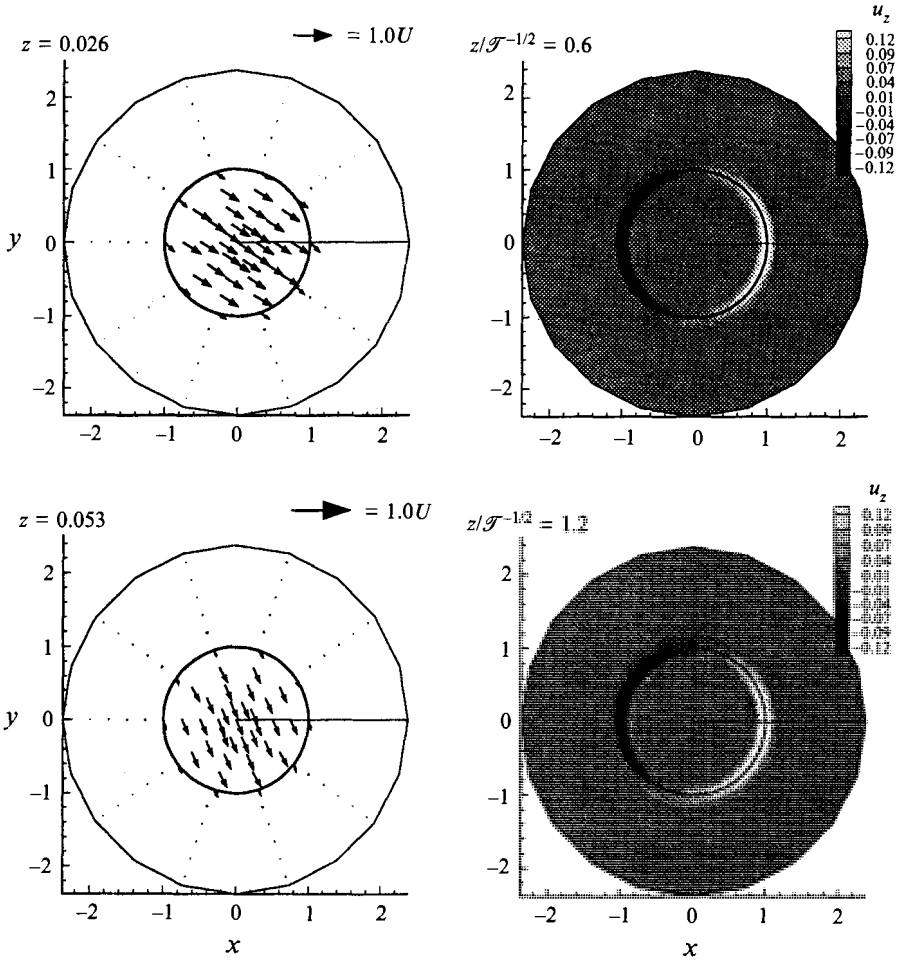

FIGURE 11. Plan view showing the Ekman layer at a sections through $z/\mathscr{T}^{-1/2} \approx 0.6, 1.2$ for $\mathscr{T} = 500$. The disk occupies the region $r < 1$ and moves from left to right. The figures on the left shows the in-plane velocity vectors; the figures on the right shows contours of the axial velocity field. The velocity vectors along the centreline spiral through nearly a full revolution as distance from the disk increases. Regions of net up-flow/down-flow occur over the leading/trailing edge. These regions rotate clockwise through 45° and develop into counter-rotating eddies (see figures 12–14.)

in the centre of the eddy is approximately 2% of the disk speed and remains nearly constant in the region ranging from $z = 5$–37. In general, the magnitude of this far-field velocity is $O(\mathscr{T}^{-1/2})$.

Figures 11–14 show eight horizontal plan-view sections at increasing distances from the disk $z/\mathscr{T}^{-1/2} = 0.6$–4.8 which illustrate the complex flow field within the Ekman layer: adjacent to the disk, the no-slip condition generates flow in the translation direction, whereas outside the Ekman layer, two counter-rotating regions cause a net flow at 45° to the translation direction (figures 8–10).

The in-plane velocity vectors near the centre of the disk spiral clockwise through almost a full revolution with increasing distance from the disk, while near the disk edge, they organize into counter-rotating eddies as the height above the disk increases. Contour plots show these eddies to be centres of axial flow into and out of the horizontal plane. The first section above the disk at $z/\mathscr{T}^{-1/2} = 0.6$ shows a

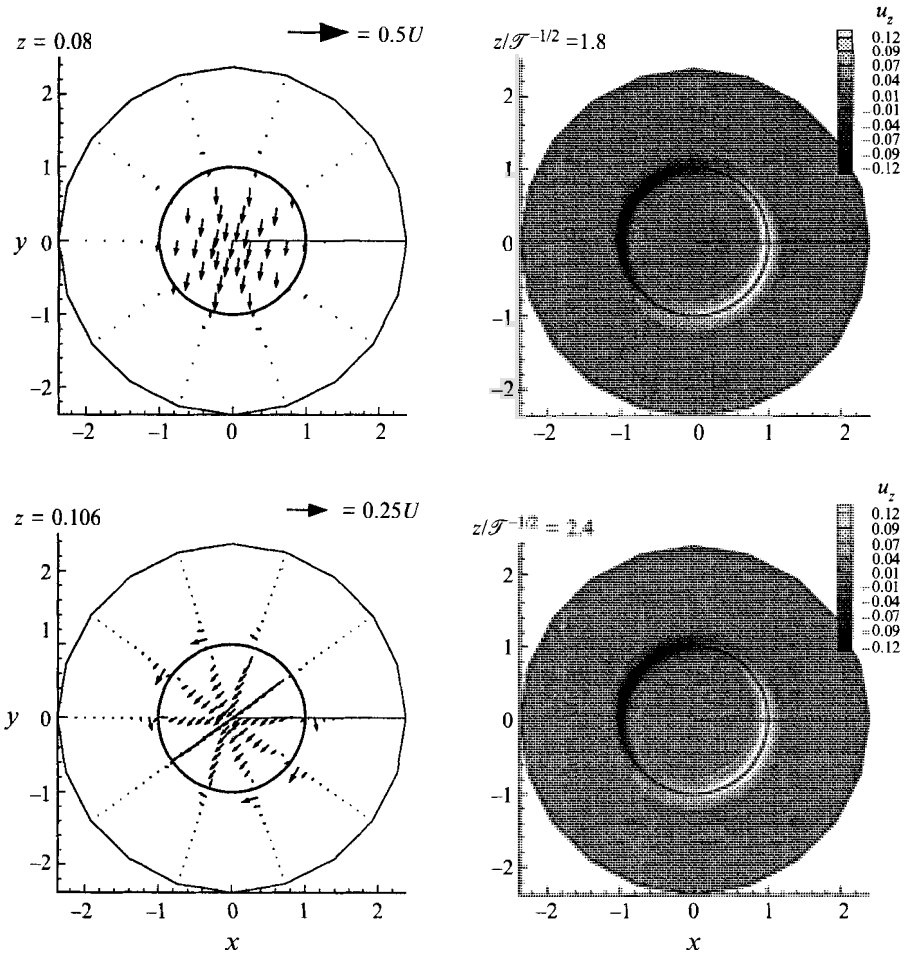

FIGURE 12. Plan view showing the Ekman layer at sections through $z/\mathscr{T}^{-1/2} = 1.8, 2.4$ for $\mathscr{T} = 500$ (see figure 11).

strong up-flow over the leading edge and a down-flow over the trailing edge of the disk. In subsequent plane sections (moving away from the disk), these regions of axial flow rotate clockwise through an angle of 45°. This net rotation is a consequence of the Coriolis force $-\Omega \wedge \boldsymbol{u}$ causing fluid elements with a radial component to turn clockwise.

4. Discussion

We conclude our discussion of the transverse translation of a rigid disk with a few general observations. Figure 15 is a schematic illustration of the instantaneous flow field generated by a disk translating perpendicular to the rotation axis of a fluid in solid-body rotation. For $\mathscr{T} \ll 1$, the flow appears as a perturbation of a Stokes flow. The velocity field is created by viscous stresses dragging fluid along with the translating disk, so that streamlines diverge in front of the translating particle and converge behind it. Such a viscous flow decays in the far field as $O(|\mathbf{x}|^{-1})$.

In contrast, for $\mathscr{T} \gg 1$ the Taylor–Proudman constraint, strictly valid for a geostrophic flow (no viscous effects), strongly influences the motion. In order to

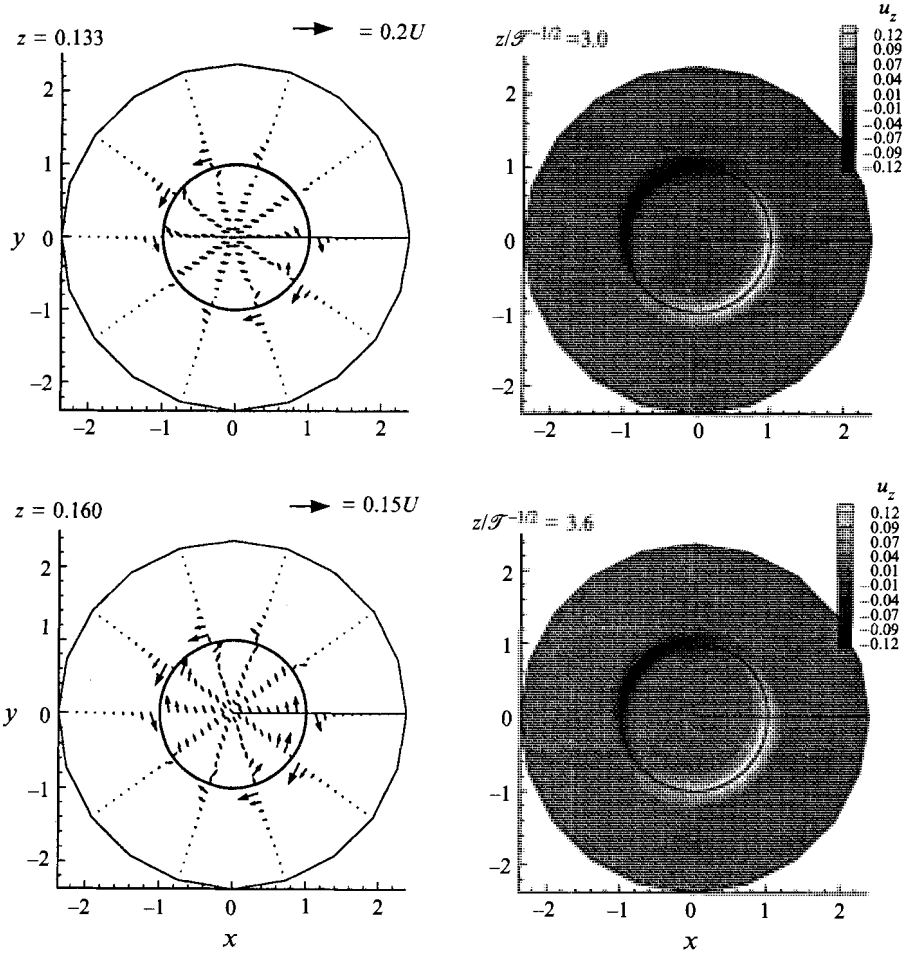

FIGURE 13. Plan view showing the Ekman layer at sections through $z/\mathscr{T}^{-1/2} = 3.0, 3.6$ for $\mathscr{T} = 500$ (see figure 11).

eliminate velocity gradients along the direction of the rotation axis, the largest $O(1)$ velocities are compressed into thin $O(\mathscr{T}^{-1/2})$ Ekman boundary layers along the disk surface. The flow within the Ekman boundary layers can be understood by considering an infinite plate translating perpendicular to the rotation axis. Figures 11–14 illustrate the Ekman spiral. As equation (3.3) demonstrates, the translating plate produces a net in-plane volume flux which is directed 45° clockwise from the translation direction. This flow feature is evident in figure 6.

The background rotation inhibits radially directed fluid motion present in the low Taylor number flows, and instead tends to cause fluid particles to move parallel to the rotation axis, as evidenced in the narrow up-flow and down-flow regions that accompany the translating disk. This weak secondary flow outside the Ekman layer is composed of two counter-rotating eddies centred over the edge of the disk and extending in a column parallel to the rotation axis as shown in figure 15. The counter-rotating eddies act together to generate a net in-plane flow directed at an angle of 45° counter-clockwise to the direction of disk translation. This secondary flow is weak, but persists for large axial distances with nearly a constant magnitudes $|u_r| \approx |u_\theta| \approx |u_z| \approx O(\mathscr{T}^{-1/2})$ over distances $z = O(\mathscr{T})$. Thus, there is a columnar character to the

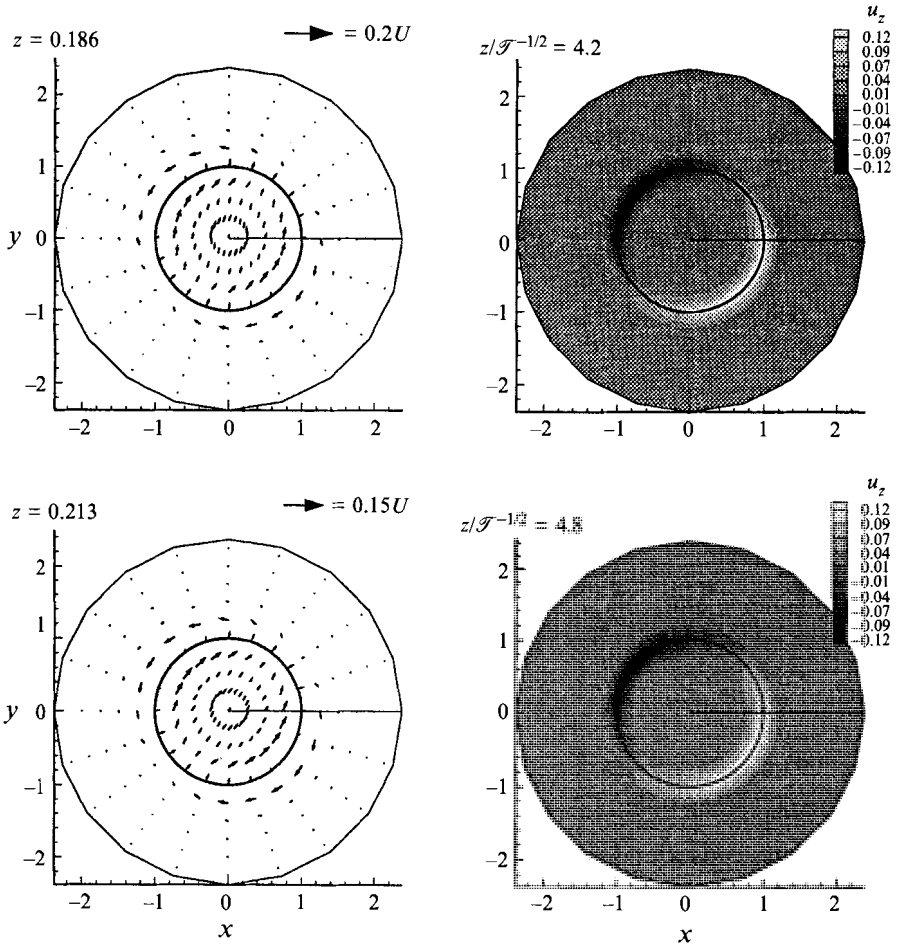

FIGURE 14. Plan view showing the Ekman layer at sections through $z/\mathscr{T}^{-1/2} = 4.2, 4.8$ for $\mathscr{T} = 500$ (see figure 11).

flow, though not the classic Taylor column (Moore & Saffman 1969*a*). In general, for $\mathscr{T} > 500$ Moore & Saffman's (1969*a*) asymptotic analysis quantitatively describes some of the detailed flow features.

The structure of the counter-rotating eddies is suggestive of the $\frac{1}{3}$-shear layer described by Moore & Saffman (1969*a*). In their analysis, a thin layer, which extends parallel to the rotation axis and is centred over the disk edge, transfers fluid in the axial direction from a source located on the disk edge. This source is fed by the Ekman layer on the disk surface. Here the two counter-rotating eddies perform the function of the $\frac{1}{3}$-layer. We can now examine how the thickness of this eddy changes with Taylor number by considering the axial velocity at a constant height through a radial slice passing through the centre of the eddy (e.g. $0 < r < 2, \theta = -\pi/4, z = 1$). We have numerically verified that the thickness over which the velocity exceeds a certain threshold (e.g. 50% of the maximum axial velocity) scales as $\mathscr{T}^{-1/3}$ and this scale is indicated in figure 15.

Finally, based upon the viscous decay of the disturbance flow field, we should expect the unbounded flow approximation to be valid provided horizontal boundaries are located at distances greater than $O(a\mathscr{T})$ from the disk.

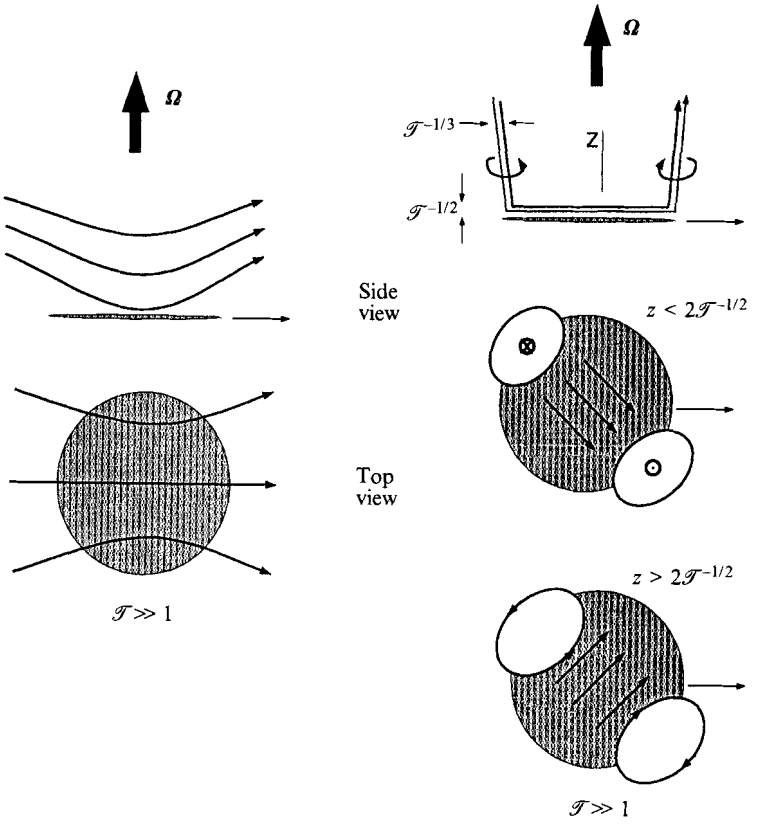

FIGURE 15. Velocity field created by a unit disk translating perpendicular to the rotation axis for $\mathcal{T} \ll 1$ and $\mathcal{T} \gg 1$. For $\mathcal{T} \ll 1$, the flow field appears as a perturbation of a Stokes flow. As the Taylor number increases, the $O(1)$ disturbance is confined to a thin $O(\mathcal{T}^{-1/2})$ Ekman boundary layer. Radial disturbances are redirected upward and downward along the axial direction, creating a secondary flow which consists of two counter-rotating eddies. The eddies, which are connected through the Ekman layers adjacent to the disk surface, generate a net volume flux away from the disk over the leading edge and toward the disk over the trailing edge. The two counter-rotating eddies create a weak net flow $O(\mathcal{T}^{-1/2})$ directed 45° counter-clockwise from the direction in which the disk is translating.

We thank Dr John D. Sherwood for many insightful conversations and Dr Steve Lucas for his help with some of the numerical issues as well as for providing routines for the integrals involving products of Bessel functions. We also thank the reviewers for their input and for suggesting the inclusion of equations (3.10) and (3.11). H. A. S. gratefully acknowledges support from NSF-Presidential Young Investigator Award CTS-8957043.

Appendix. Details of the dual integral equation formulation

This Appendix contains some of the intermediate steps in the derivation of the dual integral constraints shown in §2. The coupling coefficients $c_{ij}(k, z)$ result from regrouping the undetermined functions $\{A_1(k), A_2(k), A_3(k)\}$ in the dual integral equations into a form more suitable for solution by Tranter's method.

Based on the expressions for $\overline{U}'_{-1}$ and U_1' in equations (2.30) and (2.31), we find it

convenient to define

$$\mathscr{F}_j(k) = \frac{S_j^2\left[(S_j^2 - k^2) + \mathrm{i}2\mathscr{T}\right]}{(S_j^2 - k^2)} \qquad \text{and} \qquad \mathscr{G}_j(k) = \frac{S_j^2\left[(S_j^2 - k^2) - \mathrm{i}2\mathscr{T}\right]}{(S_j^2 - k^2)}. \tag{A 1}$$

(Note that $\mathscr{F}_j$ is not the Jacobi polynomial utilized briefly in §2.) Thus equations (2.30) and (2.31) can be expressed

$$\overline{U}'_{-1}(r,0) = -\int_0^\infty \left[\mathscr{G}_1 A_1 + \mathscr{G}_2 A_2 + \mathscr{G}_3 A_3\right] J_0(kr)\,\mathrm{d}k, \tag{A 2}$$

$$U_1'(r,0) = \int_0^\infty \left[\mathscr{F}_1 A_1 + \mathscr{F}_2 A_2 + \mathscr{F}_3 A_3\right] J_2(kr)\,\mathrm{d}k, \tag{A 3}$$

where we recall that $\pm S_j(k)$ $(j = 1,2,3)$ are the six roots of the characteristic equation

$$(S_j^2 - k^2)^3 + 4\mathscr{T}^2 S_j^2 = 0 \qquad \text{with } \mathrm{Re}\{S_j\} \geqslant 0\,. \tag{A 4}$$

This equation admits one pair of real roots labelled $\pm S_1$ and two pairs of complex-conjugate roots $\pm S_2$ and $\pm S_3 = \pm\overline{S_2}$.

The condition $W(r, z = 0) = 0$ for all r and (2.28) result in the constraint $A_1 + A_2 + A_3 = 0$. Using this constraint in (A 2) and (A 3), we can redefine the unknowns $\{A_j(k)\}$ by introducing $\Psi_1(k)$ and $\Psi_2(k)$:

$$\Psi_1 \equiv (\mathscr{G}_2 - \mathscr{G}_1)A_2 + (\mathscr{G}_3 - \mathscr{G}_1)A_3 \quad \text{and} \quad \Psi_2 \equiv (\mathscr{F}_2 - \mathscr{F}_1)A_2 + (\mathscr{F}_3 - \mathscr{F}_1)A_3, \tag{A 5}$$

from which it follows that

$$A_1 = \frac{-(\mathscr{F}_3 - \mathscr{F}_2)\Psi_1 + (\mathscr{G}_3 - \mathscr{G}_2)\Psi_2}{\Delta}, \tag{A 6}$$

$$A_2 = \frac{(\mathscr{F}_3 - \mathscr{F}_1)\Psi_1 - (\mathscr{G}_3 - \mathscr{G}_1)\Psi_2}{\Delta}, \tag{A 7}$$

$$A_3 = \frac{-(\mathscr{F}_2 - \mathscr{F}_1)\Psi_1 + (\mathscr{G}_2 - \mathscr{G}_1)\Psi_2}{\Delta}, \tag{A 8}$$

where

$$\Delta(k) \equiv \mathrm{i}4\mathscr{T}k^2 \frac{(S_2^2 - S_1^2)(S_3^2 - S_1^2)(S_3^2 - S_2^2)}{(S_1^2 - k^2)(S_2^2 - k^2)(S_3^2 - k^2)}. \tag{A 9}$$

Next we can define the coupling coefficients c_{ij} using the definitions of the complex functions $\Psi_1(k)$ and $\Psi_2(k)$ to rearrange the expressions for U_{-1} and U_{-1} given in (2.30) and (2.31). Thus

$$\overline{U}_{-1}(r,z) = -\int_0^\infty \left[\, c_{11}(k,z)\,\Psi_1(k) + c_{12}(k,z)\,\Psi_2(k)\,\right] J_0(kr)\,\mathrm{d}k, \tag{A 10}$$

$$U_1(r,z) = \int_0^\infty \left[\, c_{21}(k,z)\,\Psi_1(k) + c_{22}(k,z)\Psi_2(k)\,\right] J_2(kr)\,\mathrm{d}k, \tag{A 11}$$

where the coupling coefficients $c_{ij}(k,z)$ are given by

$$c_{11} = \frac{\mathscr{G}_1(\mathscr{F}_2 - \mathscr{F}_3)}{S_1\Delta}\,\mathrm{e}^{-S_1 z} + \frac{\mathscr{G}_2(\mathscr{F}_3 - \mathscr{F}_1)}{S_2\Delta}\,\mathrm{e}^{-S_2 z} + \frac{\mathscr{G}_3(\mathscr{F}_1 - \mathscr{F}_2)}{S_3\Delta}\,\mathrm{e}^{-S_3 z}, \tag{A 12}$$

$$c_{12} = \frac{\mathscr{G}_1(\mathscr{G}_3 - \mathscr{G}_2)}{S_1\Delta}\,\mathrm{e}^{-S_1 z} + \frac{\mathscr{G}_2(\mathscr{G}_1 - \mathscr{G}_3)}{S_2\Delta}\,\mathrm{e}^{-S_2 z} + \frac{\mathscr{G}_3(\mathscr{G}_2 - \mathscr{G}_1)}{S_3\Delta}\,\mathrm{e}^{-S_3 z}, \tag{A 13}$$

$$c_{21} = \frac{\mathscr{F}_1(\mathscr{F}_2 - \mathscr{F}_3)}{S_1\Delta}\,\mathrm{e}^{-S_1 z} + \frac{\mathscr{F}_2(\mathscr{F}_3 - \mathscr{F}_1)}{S_2\Delta}\,\mathrm{e}^{-S_2 z} + \frac{\mathscr{F}_3(\mathscr{F}_1 - \mathscr{F}_2)}{S_3\Delta}\,\mathrm{e}^{-S_3 z}, \tag{A 14}$$

$$c_{22} = \frac{\mathscr{F}_1(\mathscr{G}_3 - \mathscr{G}_2)}{S_1 \Delta} e^{-S_1 z} + \frac{\mathscr{F}_2(\mathscr{G}_1 - \mathscr{G}_3)}{S_2 \Delta} e^{-S_2 z} + \frac{\mathscr{F}_3(\mathscr{G}_2 - \mathscr{G}_1)}{S_3 \Delta} e^{-S_3 z}. \tag{A 15}$$

The unknown functions $\Psi_1(k)$ and $\Psi_2(k)$ are specified by the boundary conditions in the plane $z = 0$ as described in §2.

We can simplify the expressions derived in this section by using properties of the roots $\{S_j\}$. We have identified the roots so that S_1 is a real-valued function and $S_2, S_3 = \overline{S}_2$ form complex-conjugate pairs. (We keep only the three roots for which $\mathrm{Re}\{S_j\} \geqslant 0$ so that the coupling coefficients c_{ij} decay in the upper half-space $z > 0$.) Thus it follows that $\mathscr{G}_1 = \overline{\mathscr{F}_1}$, $\mathscr{G}_2 = \overline{\mathscr{F}_3}$, and $\mathscr{G}_3 = \overline{\mathscr{F}_2}$. Because of this result, we see that $\Delta(k)$ is a real-valued function and the coupling coefficients are related complex-conjugate pairs for which $c_{22}(k, z) = \overline{c}_{11}(k, z)$ and $c_{21}(k, z) = \overline{c}_{12}(k, z)$.

REFERENCES

ABRAMOWITZ, M. & STEGUN, I. A. 1972 *Handbook of Mathematical Functions.* Dover.

BATCHELOR, G. K. 1967 *An Introduction to Fluid Dynamics.* Cambridge University Press.

BUSH, J. W. M., STONE, H. A. & TANZOSH, J. 1995 Particle motion in rotating viscous fluids: Historical survey and recent developments. To appear in *Current Topics in the Physics of Fluids.* Research Trends, Trivandrum, India.

CHILDRESS, S. 1964 The slow motion of a sphere in a rotating, viscous fluid. *J. Fluid Mech.* **20**, 305–314.

DAVIES, P. A. 1972 Experiments on Taylor columns in rotating stratified fluids. *J. Fluid Mech.* **54**, 691–717.

DAVIS, A. M. J. 1991 Slow viscous flow due to motion of an annular disk; pressure-driven extrusion through an annular hole in a wall. *J. Fluid Mech.* **231**, 51–71.

DAVIS, A. M. J. 1992 Drag modification for a sphere in a rotational motion at small, non-zero Reynolds and Taylor numbers; wake interference and possible Coriolis effects. *J. Fluid Mech.* **237**, 13–22.

DAVIS, A. M. J. 1993 Some asymmetric Stokes flows that are structurally similar. *Phys. Fluids* A **5**, 2086–2094.

DAVIS, A. M. J. & BRENNER, H. 1986 Steady rotation of a tethered sphere at small, non-zero Reynolds and Taylor numbers: wake interference effects on drag. *J. Fluid Mech.* **168**, 151–167.

GRADSHTEYN, I. S. & RYZHIK, I. M. 1965 *Table of Integrals, Series and Products.* Academic Press.

GREENSPAN, H. P. 1968 *The Theory of Rotating Fluids.* Cambridge University Press.

HAPPEL, J. & BRENNER, H. 1973 *Low Reynolds Number Hydrodynamics.* Noordhoff, Groningen.

HERRON, I. H., DAVIS, S. H. & BRETHERTON, F. P. 1975 On the sedimentation of a sphere in a centrifuge. *J. Fluid Mech.* **68**, 209–234.

HIDE, R. 1966 On the dynamics of rotating fluids and related topics in geophysical fluid dynamics. *Bull. Am. Met. Soc.* **47**, 873–885.

HIDE, R. & IBBETSON, A. 1966 An experimental study of Taylor columns. *Icarus* **5**, 279–290.

HIDE, R. & IBBETSON, A. 1968 On slow transverse flow past obstacles in a rapidly rotating fluid. *J. Fluid Mech.* **32**, 251–272.

HOCKING, L. M., MOORE, D. W. & WALTON, I. C. 1979 The drag on a sphere moving axially in a long rotating container. *J. Fluid Mech.* **90**, 781–793.

HUGHES, B. D., PAILTHORPE, B. A. & WHITE, L. R. 1981 The translational and rotational drag on a cylinder moving in a membrane *J. Fluid Mech.* **110**, 349–372.

IMSL MATH/LIBRARY V2.0 1991 *User's Manual.* IMSL, Houston.

INGERSOLL, A. P. 1969 Inertial Taylor columns and Jupitor's Great Red Spot. *J. Atmos. Sci.* **26**, 744–752.

JACOBS, S. J. 1964 The Taylor column problem. *J. Fluid Mech.* **20**, 581–591.

KARANFILIAN, S. K. & KOTAS, T. J. 1981 Motion of a spherical particle in a liquid rotating as a solid body. *Proc. R. Soc. Lond.* A **376**, 525–544.

LIGHTHILL, M. J. 1966 Dynamics of rotating fluids: a survey. *J. Fluid Mech.* **28**, 411–431.

LUCAS, S. K. 1995 Evaluating infinite integrals involving products of Bessel functions of arbitrary order. *J. Comput. Appl. Maths* to appear.

MAGNUS, W., OBERHETTINGER, F. & SONI, R. P. 1966 *Formulas and Theorems for the Special Functions of Mathematical Physics.* Springer.

MASON, P. J. 1975 Forces on bodies moving transversely through a rotating fluid. *J. Fluid Mech.* **71**, 577–599.

MAXWORTHY, T. 1969 Some experimental observations. Appendix to D. W. Moore & P. G. Saffman. *J. Fluid Mech.* **39**, 831–847.

MOORE, D. W. & SAFFMAN, P. G. 1969*a* The flow induced by the transverse motion of a thin disk in its own plane through a contained rapidly rotating viscous liquid. *J. Fluid Mech.* **39**, 831–847.

MOORE, D. W. & SAFFMAN, P. G. 1969*b* The structure of vertical free shear layers in a rotating fluid and the motion produced by a slowly rising body. *Phil. Trans. R. Soc. Lond.* A **264**, 597–634.

RAY, M. 1936 Application of Bessel functions to the solution of problems of motion of a circular disk in viscous liquid. *Phil. Mag.* **21**, 546–564.

SAFFMAN, P. G. 1976 Brownian motion in thin sheets of viscous fluid. *J. Fluid Mech* **73**, 593–602.

SNEDDON, I. N. 1966 *Mixed Boundary Value Problems in Potential Theory.* John Wiley & Sons.

STEWARTSON, K. 1953 On the slow motion of an ellipsoid in a rotating fluid. *Q. J. Mech. Appl. Maths* **21**, 353–373.

STEWARTSON, K. 1967 On the slow transverse motion of a sphere through a rotating fluid. *J. Fluid Mech.* **30**, 357–369.

TANZOSH, J. P. 1994 Integral equation formulations of the linearized Navier-Stokes equation: applications to particle motions in rotating viscous flows. PhD dissertation, Harvard University.

TANZOSH, J. P. & STONE, H. A. 1994 Motion of a rigid particle in a rotating viscous flow: an integral equation approach. *J. Fluid Mech.* **275**, 225–256.

TANZOSH, J. P. & STONE, H. A. 1995 A general approach to analyzing the motion of a disk in a Stokes flow. *Chem. Engng Commun.* to appear.

TAYLOR, G. I. 1923 Experiments on the motion of solid bodies in rotating fluids. *Proc. R. Soc. Lond.* A **104**, 213–218.

TRANTER, C. J. 1966 *Integral Transforms in Mathematical Physics.* John Wiley & Co.

UNGARISH, M. & VEDENSKY, D. 1995 The motion of a rising disk in a rotating axially bounded fluid for large Taylor number. *J. Fluid Mech.* **291**, 1–32.

VAZIRI, A. & BOYER, D. L. 1971 Rotating flow over shallow topographies. *J. Fluid Mech.* **50**, 79–95.

VEDENSKY, D. & UNGARISH, M. 1994 The motion generated by a slowly rising disk in a rotating fluid for arbitrary Taylor number. *J. Fluid Mech.* **262**, 1–26.